A Detailed Presentation and Implementation Procedure of Axisymmetric Method of Characteristics for Rocket Nozzle Design

Written by

Kyril Palaveev
Sheffield Hallam University, Sheffield, UK

and

Dr. Torsten Schenkel
Sheffield Hallam University, Sheffield, UK

2nd September 2020

The goal of this report is to demonstrate and analyze the use of Method of Characteristics (MOC) as a design tool for the geometry of the diverging section of a rocket nozzle. The purposes of such nozzles are briefly linked to rocketry via the rocket equation and isentropic theory. Both 2D and Axisymmetric MOC procedures are derived and implemented to demonstrate the mathematical and physical differences and to prove the redundancy of 2D MOC. The Axisymmetric MOC Procedure is thoroughly reviewed and convergence studies are performed to validate suitable inputs yielding accurate nozzle geometries. Despite implementing the procedure for constructing the kernel of the characteristic net only, the philosophy and implementation of the presented Axisymmetric MOC procedure is sufficient to further refine a nozzle with the addition of new boundary conditions. The produced nozzle is validated with the use of CFD software to easily verify and discuss the outcomes of the numerical procedure.

Nomenclature

$A = Area\ [m^2]$
$X_c = At\ Combustion\ Chamber$
$X_{cn} = At\ Converging\ Nozzle$
$X_{dn} = At\ Diverging\ Nozzle$
$X_e = At\ Exhaust$
$X_t = At\ Throat$
$\beta = ConvergingAngle\ [°]$
$x, y = Coordinates\ [m]$
$\rho = Density\ [kg/m^3]$
$u, v = Fluid\ Velocity\ Components\ [m/s]$
$R = Gas\ Constant\ [J/kgK]$
$L = Length\ [m]$
$\mu = Mach\ Angle\ [°]$
$M = Mach\ Number\ [-]$
$m = Mass\ [kg]$
$\dot{m} = Mass\ Flow\ rate\ [kg/s]$
$\nu(M) = Prandtl - Meyer\ Angle\ [°]$
$p = Pressure\ [Pa]$
$r = Radius\ [m]$
$\gamma = Ratio\ of\ Specific\ Heat\ [-]$
$c_p = Specific\ Heat\ at\ Const. Pressure$
$c_v = Specific\ Heat\ at\ Const. Volume$
$I_{sp} = Specific\ Impulse\ [s]$
$a = Speed\ of\ Sound\ [m/s]$
$T = Temperature\ [K]$
$F_T = Thrust\ [N]$
$\hat{R} = Universal\ Gas\ Constant\ [J/kgK]$
$v = Vehicle\ Velocity\ [m/s]$
$\theta = Inflection\ Angle_{(MOC)}\ [°]$
$V = Velocity\ Vector_{(MOC)}\ [m/s]$

Contents

Introduction

The converging-diverging nozzle is, as suggested by its name, a hollow section of tubing with a changing cross-sectional area. De Laval in 1888[1] discovered that such geometries are useful for altering the properties of a fluid interacting internally with a nozzle. Despite its early use as a steam accelerator for steam turbines, De Laval proved a concept of isentropic theory [2], [3] – the foundation of compressible fluid dynamics. The isentropic relations are an essential foundation for every nozzle however, the quasi-1D nature of the model restrict the user from producing precise and efficient nozzle geometries. In need of more information about the flow inside a nozzle, L. Prandtl and A. Busemann, introduced the second dimension in nozzle design theory in 1929 [1]. With this planar setup, the ability of analyzing the radial (vertical) velocity component of the flow arose, replacing the disadvantaged conical nozzle with more complex geometries, most popular of which is the bell (contoured) nozzle. These complex geometries were necessary in order to produce nozzles with higher efficiencies and to eliminate the production of shockwaves inside the nozzle. Constructing a 2D flow field numerically, utilizing the Method of Characteristics (MOC)[1], is a great leap towards efficient nozzles however, this more complex mathematical model is still considered detached from the physical domain. The most basic implementation of MOC, the Planar MOC, is a dimensionless solution which is not iterable. This eliminates the ability to introduce known information and data from the physical domain to the procedure and the final results are usually with great error. A more advanced, compared to the 2D MOC, procedure is the Axisymmetric MOC which follows the same philosophy as 2D MOC however the coordinate system is cylindrical, adding more useful information to the problem. This variant of the MOC allows to iterate some of the initial parameters which would intern allow to control the output of the procedure. Both MOC procedures mentioned before are for inviscid and irrotational flows – something considered inaccurate for a nozzle in the physical domain. A procedure for rotational 3D MOC is developed however due to its complexity and infrequent usability in industry of nozzle design it is considered outside the scope of this paper.

To familiarize the reader with the structure of this paper some brief chemical theory and calculations are firstly presented in order to obtain the thermofluid properties of the working fluid. This section of the report also acquaints the reader with justification for the chosen reactants and initial specifications for the nozzle which is assumed to be part of a rocket motor assembly. The base parameters of the nozzle are then obtained with the use of isentropic theory which automatically yields a conical nozzle. Following the conical nozzle is the introduction of the philosophy and derivation of 2D Method of Characteristics. The procedure is then implemented manually and a nozzle is constructed to demonstrate its redundancy in rocket nozzle design. The already derived 2D MOC equations are then modified for a cylindrical coordinate system and those partial differential equations are solved to an algebraic form so that they are numerically solvable by implementing them in a computer programme

written in Python 3.7. Once the nozzle contour coordinates are obtained they are discussed and the geometry is validated using Ansys CFD.

Chemical Kinetics

Differing from De Laval's steam nozzle, the propelling gas of a rocket is a result of combustion. Requiring an oxidizer and fuel and also given the existence of many possible options for each of the needed components for combustion it would be unreasonable to shift the focus from a nozzle design procedure. Therefore this paper will adopt a seemingly popular oxidizer and fuel for demonstration purposes. Liquid oxygen (O_2) and methane (CH_4) are fluidic, non-hypergolic, and environmentally friendly reactants with high availability and low risk factors. In chemistry, the term "*chemical equilibrium*" [4] refers to the ratio of these two compounds when they fully react. This mixture is known as the stoichiometric ratio:

$$CH_4 + 2O_2 \rightarrow CO_2 + 2H_2O \tag{1}$$

Although the expression above seems logical to implement, in practice, rocket motors burn an *optimum mixture ratio* [5] which is richer in oxidizer than the stoichiometric mixture ratio. The optimum mixture ratio is desirable as it produces a heavier exhaust gas, increasing the inertia of the working fluid and thus increasing thrust. Unfortunately the optimum mixture ratio cannot be calculated accurately analytically. This is due to the generation of more complex compounds in the product than those described in equation (1) and due to the amount of variables that differ for different oxidizer to fuel (O/F) ratios. A numerical procedure for computing the fluid's properties at different mixture ratios exists. This numerical procedure is implemented into the NASA CEA[6] (Chemical Equilibrium with Applications) software and is used for this report to determine the most efficient O/F ratio. Prior to reviewing the data from the numerical chemical analysis, the reader is acquainted with the derivation of a parameter known as the *specific impulse* that is essential to linking chemical kinetics with motor performance.

First and foremost the Tsiolkovsky equation[7] is presented:

$$\Delta v = u_{eq} \ln\left(\frac{m_0}{m_f}\right) \tag{2}$$

From a thermofluid perspective the equivalent exhaust velocity (u_{eq}) is defined as:

$$u_{eq} = \frac{(p_e - p_{atm})A_e}{\dot{m}} + u_e \tag{3}$$

From the thrust equation[1]:

$$F_T = \dot{m}u_e + (p_e - p_{atm})A_e \tag{4}$$

Dividing the right sides of equation (3) by the mass flow rate reveals:

$$\dot{m}u_{eq} = (p_e - p_{atm})A_e + \dot{m}u_e \tag{5}$$

Comparing equations (4) and (5) indicates that:

$$F_T = \dot{m}u_e + (p_e - p_{atm})A_e = \dot{m}u_{eq} \tag{6}$$

At this stage a crucial design decision is made. Rocket nozzles can operate in one of the three following states. They can be over-expanded – when the ambient pressure is greater than the exhaust pressure; under-expanded – when the ambient pressure is lower than the exhaust pressure; and perfectly-expanded – when the ambient pressure is equal to the exhaust pressure. In over-expanded nozzles an adverse pressure gradient is present thus forcing the flow to separate from the wall. Turbulent flows are known for their chaotic behavior therefore undesirable for rocket nozzles. Having an atmospheric pressure equal to the exhaust pressure is ideal and nozzles are usually designed around this parameter. However, as rockets ascent the atmospheric pressure decreases putting the nozzle in the second state of expansion. When under-expanded the efficiency of the nozzle decreases but the overall thrust output increases as the equivalent velocity increases. A conclusion is therefore made that nozzles are designed to be perfectly-expanded at the highest ambient pressure in which they operate. Assuming that the rocket on which this nozzle is mounted takes-off at Mean Sea Level (MSL), the highest ambient pressure would be 101325 [Pa]. Equating this value to the exhaust pressure would yield:

$$F_T = \dot{m}u_e + 0 = \dot{m}u_{eq} + 0 \tag{7}$$

$$\therefore u_e = u_{eq} \tag{8}$$

The impulse in physics is classified as the change in force over time. Known more commonly in rocketry as the total impulse it can be mathematically expressed as:

$$I = \int F_T \, dt \tag{9}$$

Substituting equation (7) into equation (9):

$$I = \int \dot{m}u_e \, dt \tag{10}$$

Since the exhaust velocity is a constant and the mass flow rate is a function of time:

$$I = mu_e \tag{11}$$

The specific impulse is then defined as the total impulse over the accelerated weight. From Newton's 2nd Law and equation (11):

$$I_{sp} = \frac{I}{mg} \tag{12}$$

Substituting equation (11) into equation (12):

$$I_{sp} = \frac{u_e}{g} \tag{13}$$

The exhaust velocity, as previously mentioned, varies with the mass of the compounds. As weight increases, velocity decreases but inertia increases. This suggests the parabolic nature of the specific impulse when examined as a function of molar mass. Since the oxidizer and fuel have different masses and mass fractions, altering the oxidizer to fuel ratio (O/F) will directly influence the molar mass of the overall working fluid.

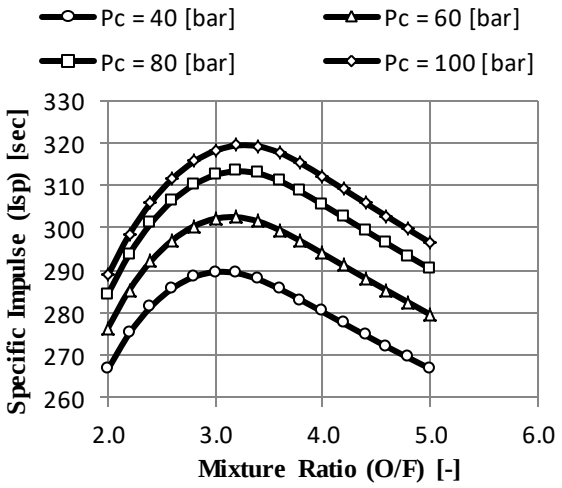

(Graph 4.1) – Specific impulse variation over mixture ratio of liquid methane and liquid oxygen. (Ref. [6])

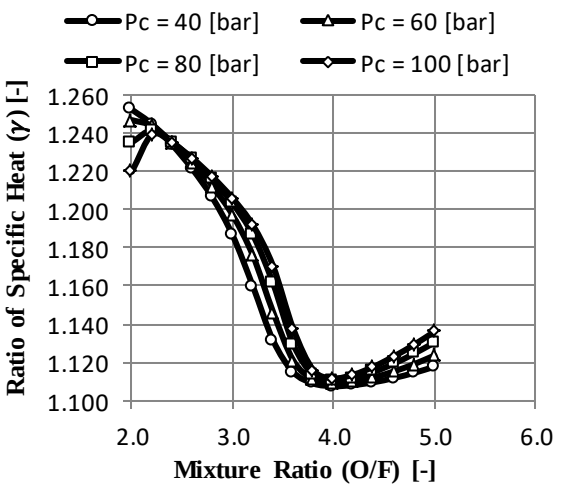

(Graph 4.2) – Ratio of specific heat variation over mixture ratio of liquid methane and liquid oxygen. (Ref. [6])

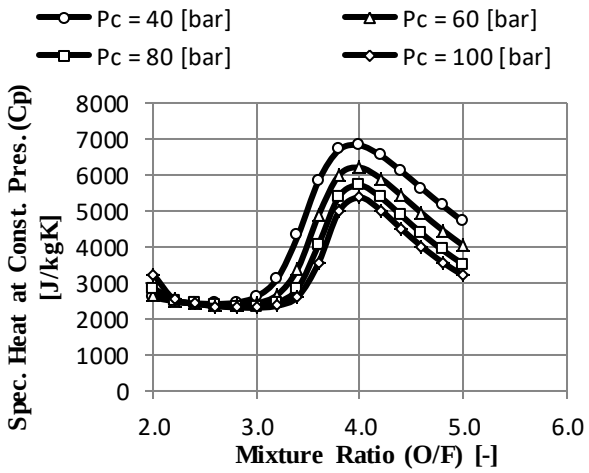

(Graph 4.3) – Specific heat at constant pressure variation over mixture ratio of liquid methane and liquid oxygen. (Ref. [6])

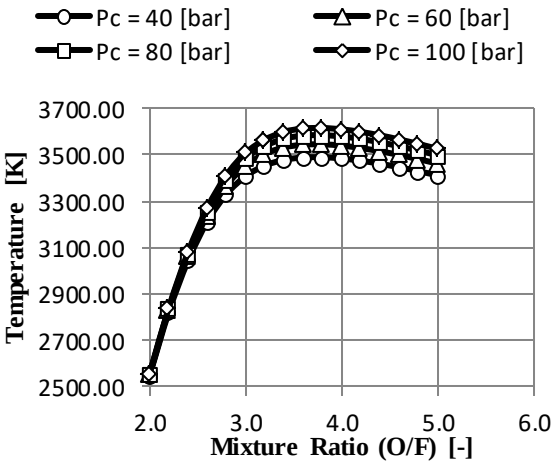

(Graph 4.4) – Combustion temperature variation over mixture ratio of liquid methane and liquid oxygen. (Ref. [6])

Strong mathematical evidence from Graph 4.1 suggests that the optimum mixture ratio is approximately 3.2. Graphs 4.2, 4.3, and 4.4 however, peak at a mixture ratio of 4.0 and this is due to the combustion efficiency. The ratio of specific heat is lowest at the highest combustion efficiency which is not necessarily a desired quality since the higher the combustion efficiency the higher the combustion temperature and from a practical standpoint the combustion chamber becomes less cost-effective. For this nozzle design from the graphs above the presented in table 5.1 properties are selected.

Combustion Pressure (p_c) $[Pa]$					
8 $[MPa]$					
O/F Ratio	**Ratio of Specific Heat (γ)**	**Specific Gas Constant (R) $[J/kgK]$**	**Specific Heat at Constant Pressure (c_p) $[J/kgK]$**	**Combustion Chamber Temperature $[K]$**	**Specific Impulse (I_{sp}) $[sec]$**
3.2	1.1877	382.08	2428.60	3538.69	313.303

(Table 5.1) – Gas properties of nozzle fluid for chosen mixture ratio

This concludes the section on chemical kinetic. The obtained parameters are essential for the next section of the report.

Isentropic Theory

Compressible flow can be algebraically expressed with the isentropic equations which demonstrate the relationship between gas properties at two locations and the Mach number of the working fluid. To understand the limitations, boundaries, and outcomes of isentropic theory the mass flow rate, equation (20) and the speed of sound equation (21) are examined.

$$\dot{m} = \rho A u = constant \tag{14}$$

$$a = \sqrt{\gamma R T} \tag{15}$$

Since the velocity in equation (14) can be expressed as Mach number:

$$M = \frac{u}{a} \tag{16}$$

Equation (14) is written in the form:

$$\dot{m} = \rho A M \sqrt{\gamma R T} \tag{17}$$

The ideal gas Law is used to represent the ideal gas constant as follows:

$$R = \frac{\gamma p}{\rho T} \tag{18}$$

The equation for continuous flow and the energy equation [3] yield:

$$\frac{1}{2} M^2 a^2 + c_p T = constant \tag{19}$$

Where it is important to note that:

$$R = c_p - c_v \tag{20}$$

$$\gamma = \frac{c_p}{c_v} \tag{21}$$

From equations (19), (20), and (21) the following equation yields:

$$\frac{1}{2} u^2 + \frac{a^2}{\gamma - 1} = constant \tag{22}$$

Since equations (22) and/or (19) are constant along a streamline the isentropic ratios are derived:

$$\frac{p_x}{p_0} = \left(1 + \frac{\gamma - 1}{2} M_x^2\right)^{\frac{\gamma}{\gamma - 1}} \tag{23}$$

$$\frac{T_x}{T_0} = \left(1 + \frac{\gamma - 1}{2} M_x^2\right) \tag{24}$$

$$\frac{\rho_x}{\rho_0} = \left(1 + \frac{\gamma - 1}{2} M_x^2\right)^{-\frac{1}{\gamma - 1}} \tag{25}$$

From thermofluid dynamics, the term “isentropic” refers to the mathematical model of a fluid that is adiabatic and reversible. The adiabatic process is associated with its unrealistic lack of heat and mass transfer outside the analyzed system. This allows for the constant mass flow rate statement made earlier. Furthermore the derivation of the isentropic relations includes the assumption that the entropy along a streamline is constant. The term “reversible” indicates that isentropic theory does not account for shockwaves which are usually observed in less complex nozzle geometries.

From the chosen combustion pressure and the CEA-calculated combustion temperature and gas properties the isentropic properties of the nozzle are calculated at the chamber, throat and exhaust (Table 8.1). It is important to note that the used isentropic process utilizes constant gas properties which create a less accurate model than the “frozen” and “equilibrium” processes which are known for a variable gas constant.

	Combustion Chamber (X_c)	Throat (X_t)	Exhaust (X_e)
Pressure [Pa]	**8 000 000.0**	4 536 585.5	**101 325.0**
Temperature [K]	**3538.69**	3 236.88	1 779.96
Density [kg/m^3]	5.92	3.67	0.15
Mach number [$-$]	**0.000**	**1.000**	3.2554
Velocity [m/s]	**0.0**	941.4	2923.0

(Table 8.1) – Results from isentropic calculations for a converging-diverging nozzle. Note: Values in bold are known values (boundary conditions).

The area-Mach number relationship (equation (27)) and the mass flow rate equation (equation (14)) are used to determine the areas and radii of the throat and exhaust of the nozzle (Table 9.1).

$$\frac{A_e}{A_t} = \left(\frac{\gamma+1}{2}\right)^{-\frac{\gamma+1}{2(\gamma-1)}} \frac{\left(1+\frac{\gamma-1}{2}M_e^2\right)^{\frac{\gamma+1}{2(\gamma-1)}}}{M_e} \quad (27)$$

The combustion chamber area cannot be evaluated using isentropic theory due to the zero-velocity assumption at that point. Through experimental data is has been determined that a suitable combustion chamber area is equal to 3 times that of the throat [8].

	Combustion Chamber (X_c)	Throat (X_t)	Exhaust (X_e)
Area [m^2]	0.002310	0.000770	0.007841
Radius [m]	0.027119	0.01566	0.049958

(Table 9.1) – Results of area and radii for critical segments of a converging-diverging nozzle

The isentropic ratios are then plotted as functions of Mach number (graph 10.1). The area ratio is plotted in graph 10.2.

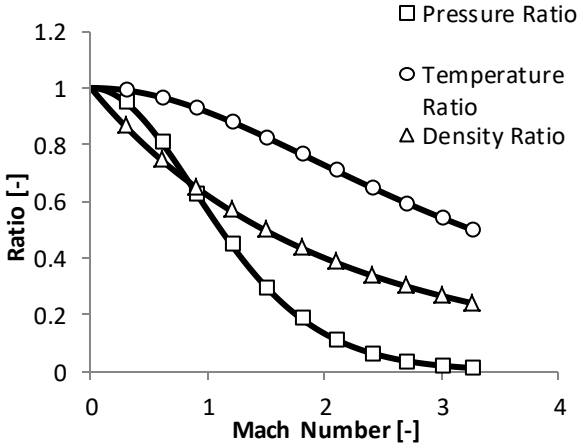

(Graph 10.1) – Isentropic ratios versus Mach number for converging-diverging nozzle

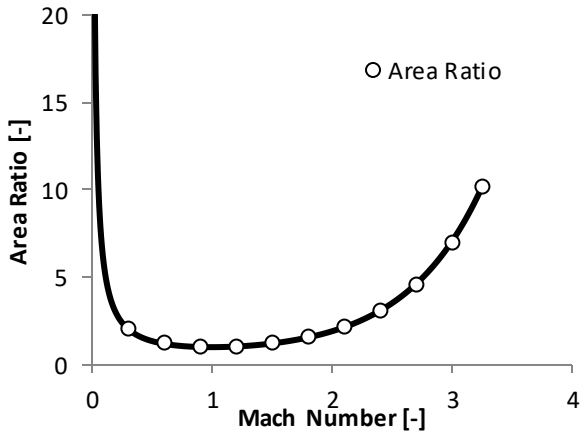

(Graph 9.2) – Area ratio versus Mach number for converging-diverging nozzle

With the use of the isentropic process the critical areas of the nozzle are found (i.e. chamber, throat, and exhaust area). These are crucial boundary conditions for the upcoming numerical design procedure as all MOC procedures are detached from the area-Mach-number relationship and therefore one cannot design a nozzle contour using MOC without having a finite value for the exhaust radius to iteratively steer the numerical solution to.

Method of Characteristics: Introduction

A technique considered most popular in computational fluid dynamics is used to numerically compute the needed nozzle contour to optimize the behavior of the fluid [1,9,10]. Some basic conservation laws of fluid dynamics state that flows in different regimes behave differently and these laws are in the form of partial differential equations (PDEs), meaning that they have multiple independent variables. A general description of the method of characteristics (MOC) is a technique for solving the PDEs in question to obtain sets of ordinary differential equations (ODEs) which are more easily solvable. However, a PDE cannot be reduced to an ODE for any input – the spatial locations (i.e. coordinates in a fluid field) on which the PDEs can become ODEs are known as characteristic curves (i.e. characteristics). In essence, the goal of the MOC procedures is to numerically compute the location of these characteristics and where they intersect. The means of computing those locations are presented in the following sections of this paper.

Nozzle flows go through three out of the four flow regimes that are currently explained with the aid of partial differential equations. In the converging section of the nozzle the flow is initially in the subsonic regime. The PDEs describing the behavior of subsonic flows are elliptical, indicating that the solutions would be imaginary as the discriminant of the differential equations would be negative (i.e. $D = \sqrt{-\infty < a < 0}$). When the flow reaches the throat region of the nozzle, the flow reaches sonic speeds – Mach number is 1. Therefore the discriminant of the PDE describing the flow would be zero indicating a parabolic solution with two identical real solutions (i.e. $D = \sqrt{0} \quad \therefore x_1 = x_2$). Increasing the Mach number even further yields hyperbolic solutions – ones that have two distinct and real solutions. The number and type of solutions in fact indicate the number of characteristic lines passing though one fluid parcel (vector point) with some coordinates. For subsonic flows (elliptical PDEs) those characteristic lines are imaginary and cannot be plotted in a real 2D Cartesian coordinate system. Furthermore the MOC is a pseudo-graphical method for obtaining a nozzle contour and constructing a converging section using this method would be difficult and in most cases impractical as simpler methods for constructing a subsonic contour exist. The scope of implementation of the Method of Characteristics is from the throat to the exhaust of the nozzle since the differential equations are hyperbolic and are also classified as first order partial differential equations – the type of PDEs that MOC is typically applied to. More in-depth explanations of the philosophy of the Method of Characteristics and solutions of PDEs can be found in textbooks and papers such as in reference [1, 10, and 11]

2D Method of Characteristics: Derivation

Defining a flow field begins with setting a notation for the fluid parcels' spatial properties. Any vector is considered to have three velocity components. Along the x-axis the velocity vector has a component u, along the y-axis the velocity vector has a velocity component v, and along the z-axis – a velocity

component w. From basic vector theory the resultant of u, v, and w yields the direction and magnitude of the vector.

Irrotationality

Irrotationality of the vector V is mathematically expressed as:

$$\underline{\nabla} \times \underline{V} = 0 \tag{28}$$

$$Curl(V) = \underline{\nabla} \times \underline{V} = \begin{vmatrix} \hat{\imath} & \hat{\jmath} & \hat{k} \\ \frac{\partial}{\partial x} & \frac{\partial}{\partial y} & \frac{\partial}{\partial z} \\ u & v & w \end{vmatrix} \tag{29}$$

Solving the determinant using Cramer's rule:

$$\underline{\nabla} \times \underline{V} = \hat{\imath}\left(\frac{\partial}{\partial y}w - \frac{\partial}{\partial z}v\right) - \hat{\jmath}\left(\frac{\partial}{\partial x}w - \frac{\partial}{\partial z}u\right) + \hat{k}\left(\frac{\partial}{\partial x}v - \frac{\partial}{\partial y}u\right) = 0 \tag{30}$$

Since equation (41) is equal to zero, the terms in the brackets (irrotationality conditions) must be equal:

$$\frac{\partial}{\partial y}w = \frac{\partial}{\partial z}v \tag{31}$$

$$\frac{\partial}{\partial x}w = \frac{\partial}{\partial z}u \tag{32}$$

$$\frac{\partial}{\partial x}v = \frac{\partial}{\partial y}u \tag{33}$$

Momentum Equation

By substituting the vector V into Euler's equation:

$$\rho\frac{DV}{Dt} = -\nabla p \tag{34}$$

Where the material derivative:

$$\frac{D}{Dt} \equiv \frac{\partial}{\partial t} + u\frac{\partial}{\partial x} + v\frac{\partial}{\partial y} + w\frac{\partial}{\partial z} = \frac{\partial}{\partial t} + (\nabla \cdot \underline{V}) \tag{35}$$

$$\rho u\frac{\partial u}{\partial x} + \rho v\frac{\partial v}{\partial y} + \rho w\frac{\partial w}{\partial z} = -\frac{\partial p}{\partial x} \tag{36}$$

Substituting the irrotationality conditions and solving for each component (x, y, and z):

$$-\frac{\partial p}{\partial x}dx = \frac{1}{2}\rho\frac{\partial u^2}{\partial x}dx + \frac{1}{2}\rho\frac{\partial v^2}{\partial x}dx + \frac{1}{2}\rho\frac{\partial w^2}{\partial x}dx \tag{37}$$

$$-\frac{\partial p}{\partial y}dy = \frac{1}{2}\rho\frac{\partial u^2}{\partial y}dy + \frac{1}{2}\rho\frac{\partial v^2}{\partial y}dy + \frac{1}{2}\rho\frac{\partial w^2}{\partial y}dy \tag{38}$$

$$-\frac{\partial p}{\partial z}dz = \frac{1}{2}\rho\frac{\partial u^2}{\partial z}dz + \frac{1}{2}\rho\frac{\partial v^2}{\partial z}dz + \frac{1}{2}\rho\frac{\partial w^2}{\partial z}dz \tag{39}$$

Adding equations (37), (38), and (39) together yields:

$$\begin{aligned}-\left(\frac{\partial p}{\partial x}dx + \frac{\partial p}{\partial y}dy + \frac{\partial p}{\partial z}dz\right) = {} & \frac{1}{2}\rho\frac{\partial u^2}{\partial x}dx + \frac{1}{2}\rho\frac{\partial v^2}{\partial x}dx + \frac{1}{2}\rho\frac{\partial w^2}{\partial x}dx + \\ & \frac{1}{2}\rho\frac{\partial u^2}{\partial y}dy + \frac{1}{2}\rho\frac{\partial v^2}{\partial y}dy + \frac{1}{2}\rho\frac{\partial w^2}{\partial y}dy + \\ & \frac{1}{2}\rho\frac{\partial u^2}{\partial z}dz + \frac{1}{2}\rho\frac{\partial v^2}{\partial z}dz + \frac{1}{2}\rho\frac{\partial w^2}{\partial z}dz\end{aligned} \tag{40}$$

Knowing that:

$$\underline{V}^2 = u^2 + v^2 + w^2 \tag{41}$$

Equation (40) reduces to:

$$-\left(\frac{\partial p}{\partial x}dx + \frac{\partial p}{\partial y}dy + \frac{\partial p}{\partial z}dz\right) = \frac{1}{2}\rho\frac{\partial V^2}{\partial x}dx + \frac{1}{2}\rho\frac{\partial V^2}{\partial y}dy + \frac{1}{2}\rho\frac{\partial V^2}{\partial z}dz \tag{42}$$

Since on both sides of equation (42) all components are present the PDE is classified as an exact differential. It can therefore be written in the form:

$$dp = -\frac{1}{2}\rho dV^2 = -\rho V dV \tag{43}$$

Known as the Momentum equation, equation (43) is one of the three conditions needed to define the boundary conditions for Method of Characteristics.

Continuity Equation

For any 3-dimensional fluid parcel, its mass can be mathematically expressed as:

$$m = \rho\underline{V} = \int \rho dV = \int \rho\, dx\, dy\, dz \tag{44}$$

Typically, the continuity equation is expressed in the time domain therefore a time derivative is introduced in the conservation of mass equation. However, in the case of this paper, steady-state flow is assumed therefore in need of a special form of the continuity equation. This simplification allows the assumption that through time, the mass entering or leaving the system through any of the surfaces of the fluid parcel is constant:

$$\frac{\partial}{\partial x}\rho u + \frac{\partial}{\partial y}\rho v + \frac{\partial}{\partial z}\rho w = 0 \tag{45}$$

Simplifying equation (45):

$$\nabla \cdot (\rho u + \rho v + \rho w) = 0 \tag{46}$$

$$\nabla \cdot \rho(u + v + w) = 0 \tag{47}$$

$$\nabla \cdot \rho \underline{V} = 0 \tag{48}$$

Velocity Potential Equation

Defining the velocity potential function (Φ) as:

$$u = \frac{\partial \Phi}{\partial x} \qquad v = \frac{\partial \Phi}{\partial y} \qquad w = \frac{\partial \Phi}{\partial z} \tag{49}$$

Recall and substitute equation (49) into the momentum equation (43):

$$dp = -\rho d\left(\frac{\Phi_x^2 + \Phi_y^2 + \Phi_z^2}{2}\right) \tag{50}$$

The differential form of the speed of sound expression is:

$$a^2 = \frac{dp}{d\rho} \tag{51}$$

Substituting equation (51) into (50) yields:

$$d\rho = -\frac{\rho d}{a^2}\left(\frac{\Phi_x^2 + \Phi_y^2 + \Phi_z^2}{2}\right) \tag{52}$$

Taking the derivative for each direction of equation (52):

$$\frac{\partial \rho}{\partial x} = -\frac{\rho}{a^2}\left(\Phi_{xx}\Phi_x + \Phi_{yx}\Phi_y + \Phi_{zx}\Phi_z\right) \tag{53}$$

$$\frac{\partial \rho}{\partial y} = -\frac{\rho}{a^2}\left(\Phi_{xy}\Phi_x + \Phi_{yy}\Phi_y + \Phi_{zy}\Phi_z\right) \tag{54}$$

$$\frac{\partial \rho}{\partial z} = -\frac{\rho}{a^2}\left(\Phi_{xz}\Phi_x + \Phi_{yz}\Phi_y + \Phi_{zz}\Phi_z\right) \tag{55}$$

Substituting equation (49) into the continuity equation (equation (48)):

$$\frac{\partial}{\partial x}\rho\Phi_x + \frac{\partial}{\partial y}\rho\Phi_y + \frac{\partial}{\partial z}\rho\Phi_z = 0 \tag{56}$$

$$\rho\left(\Phi_{xx} + \Phi_{yy} + \Phi_{zz}\right) + \Phi_x\frac{\partial}{\partial x} + \Phi_y\frac{\partial}{\partial y} + \Phi_z\frac{\partial}{\partial z} = 0 \tag{57}$$

Equations (53), (54), and (55) are substituted into equation (57):

$$\left(1 - \frac{\Phi_x^2}{a^2}\right)\Phi_{xx} + \left(1 - \frac{\Phi_y^2}{a^2}\right)\Phi_{yy} + \left(1 - \frac{\Phi_z^2}{a^2}\right)\Phi_{zz} - \frac{2\Phi_x\Phi_y}{a^2}\Phi_{xy} - -\frac{2\Phi_x\Phi_z}{a^2}\Phi_{xz} - -\frac{2\Phi_z\Phi_y}{a^2}\Phi_{zy} = 0 \tag{58}$$

Since this paper will not address any 3-dimensional flow fields, a 2-dimensional version of the velocity potential equation is presented:

$$\left(1 - \frac{\Phi_x^2}{a^2}\right)\Phi_{xx} - \frac{2\Phi_x\Phi_y}{a^2}\Phi_{xy} + \left(1 - \frac{\Phi_y^2}{a^2}\right)\Phi_{yy} = 0 \tag{59}$$

Summary of Equations

For convenience table 14.1 summarizes the previously derived equations:

Irrotationality	$\underline{\nabla} \times \underline{V} = 0$
Momentum Equation	$dp = -\rho \underline{V} dV$
Continuity Equation	$\nabla \cdot \rho\underline{V} = 0$
Velocity Potential Equation	$\left(1 - \frac{\Phi_x^2}{a^2}\right)\Phi_{xx} - \frac{2\Phi_x\Phi_y}{a^2}\Phi_{xy} + \left(1 - \frac{\Phi_y^2}{a^2}\right)\Phi_{yy} = 0$

(Table 14.1) – Summary of differential equations for 2D MOC

2D Method of Characteristics

Characteristics Equation

From the previously derived equations we can treat the following terms as displayed:

$$\Phi_x = u \qquad \Phi_y = v \tag{60}$$

$$(dx)\Phi_{xx} + (dy)\Phi_{xy} = du \qquad (dx)\Phi_{xy} + (dy)\Phi_{yy} = dv \tag{61}$$

Equations (60) and (61) are substituted into the velocity potential equation:

$$\left(1 - \frac{u^2}{a^2}\right)\Phi_{xx} - \frac{2uv}{a^2}\Phi_{xy} + \left(1 - \frac{v^2}{a^2}\right)\Phi_{yy} = 0 \tag{62}$$

From equations (61) and (62) two 3 by 3 determinants are created to solve for Φ_{xy}:

$$\Phi_{xy} = \frac{A}{B} = \frac{\begin{vmatrix} 1 - \frac{u^2}{a^2} & 0 & 1 - \frac{v^2}{a^2} \\ dx & du & 0 \\ 0 & dv & dy \end{vmatrix}}{\begin{vmatrix} 1 - \frac{u^2}{a^2} & -\frac{2uv}{a^2} & 1 - \frac{v^2}{a^2} \\ dx & dy & 0 \\ 0 & dx & dy \end{vmatrix}} \tag{63}$$[1]

Thoroughly explained in multiple textbooks and papers [1, 9, 10, 11], a specific condition for determinant A and B exist. Valid results wouldn't yield from equation (63) if the denominator is different than zero since different inputs for dx and dy would yield identical values for du and dv. However, for a denominator of 0 in equation (63), the solution would be infinite which is untrue since the physical domain suggests the possibility of a finite solution. To force the solution of equation (63) to be finite, determinant A must also be 0. This indicates that the solution for Φ_{xy} must be indeterminate to yield the location at which characteristic lines cross.

From equation (62), for $B = 0$, the determinant yields a quadratic equation describing the slope of the characteristic lines:

$$\left(1 - \frac{u^2}{a^2}\right)\left(\frac{dy}{dx}\right)_{char}^{2} - \frac{2uv}{a^2}\left(\frac{dy}{dx}\right)_{char} + \left(1 - \frac{v^2}{a^2}\right) = 0 \tag{64}$$

Using the quadratic formula on equation (64):

$$\left(\frac{dy}{dx}\right)_{char} = \frac{-\frac{2uv}{a^2} \pm \sqrt{\frac{2uv}{a^2} - 4\left(1 - \frac{u^2}{a^2}\right)\left(1 - \frac{v^2}{a^2}\right)}}{2\left(1 - \frac{u^2}{a^2}\right)} \tag{65}$$

Through algebraic manipulations and trigonometric functions, equation (65) is reduced to its simplest form:

$$\left(\frac{dy}{dx}\right)_{char} = \tan(\theta \mp \mu) \tag{66}$$

where θ is the angle between the velocity vector and the x-axis and μ – the Mach angle – is the angle between the velocity vector and the characteristic lines – therefore also called Mach lines (Figure 15.1). It is obvious that two solutions exist for a set of angles. $\theta + \mu$ is known as a left-running characteristic (C_+) and $\theta - \mu$ – a right-running characteristic (C_-).

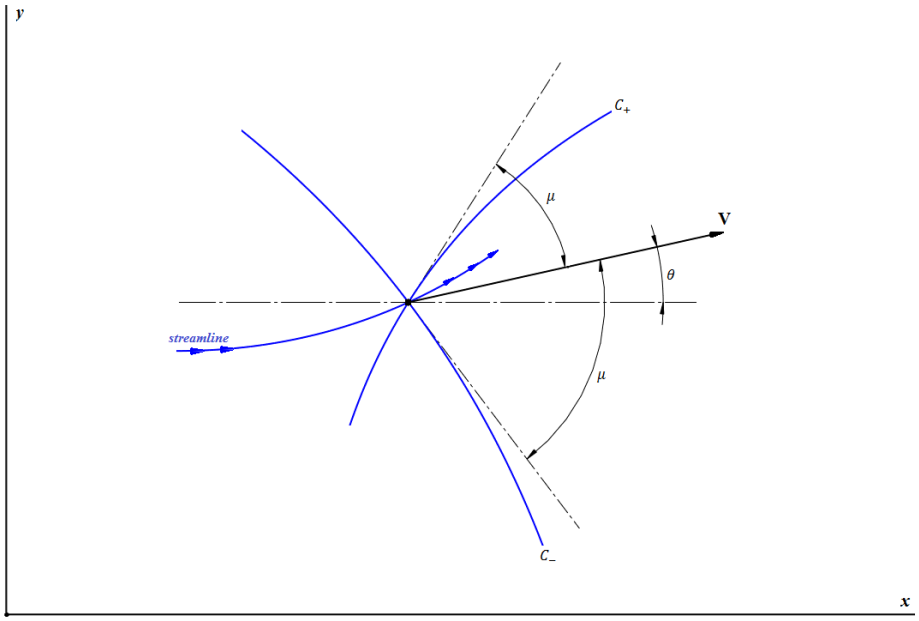

(Figure 15.1) – A graphical representation of characteristic lines and a stream line in a Cartesian coordinate system

Compatibility Equation

The characteristics equation informs the user on the slope of a characteristic line. Now the focus is on how the slope changes with respect to space. In figure 15.1 it is shown that characteristic lines are curved. The compatibility equation is the solution of determinant A when it is equal to 0.

Using Cramer's rule on the numerator in equation (63) gives:

$$\left(1 - \frac{u^2}{a^2}\right) dudy + \left(1 - \frac{v^2}{a^2}\right) dxdv = 0 \tag{67}$$

Rearranging:

$$-\frac{\left(1-\frac{u^2}{a^2}\right)}{\left(1-\frac{v^2}{a^2}\right)}\left(\frac{dy}{dx}\right)_{char}=\frac{dv}{du} \tag{68}$$

Again through algebraic and trigonometric manipulations equation (68) reduces to the compatibility equation:

$$d\theta = \mp\frac{\sqrt{M^2-1}}{V}\,dV \tag{69}$$

As previously said, the compatibility equation describes the change in resultant angle ($d\theta$) with respect to the change in resultant velocity (dV). Equation (69) is also identical to the equation developed by Prandtl and Meyer used to mathematically model expansion waves. Integrating both sides of equation (69) with some limits yields the Prandtl-Meyer function ($\nu(M)$) from which the compatibility equation is reduced to:

$$\theta \mp \nu = consant \tag{70}$$

For $\theta+\nu$ the constant is known as K_- and runs along the C_- characteristics. For $\theta-\nu$ the constant is K_+ and runs along the C_+ characteristic. It is of great importance that the reader acknowledges that equation (69) is dimensionless. This indicates that there is no requirement for previously obtained information and values which makes 2D MOC a rarely used method in the practical design of nozzles. Other MOC procedures, one of which is later introduced, have different compatibility equations eliminating the issue with dimensionless nozzles.

Methodology

To utilize the characteristic and compatibility equations boundary conditions are needed to initiate a calculation. To demonstrate the implementation of 2D MOC, 8 characteristic lines are calculated and plotted. The reader however, must be aware that in reality the number of characteristic lines is infinite. This indicates that with an increase in the number of characteristic lines the accuracy of the nozzle contour increases.

The two crucial boundary conditions for a 2D MOC minimum-length nozzle are the maximum initial expansion angle – θ_{max} located at the throat and the exhaust angle – θ_e (Figure 17.1).

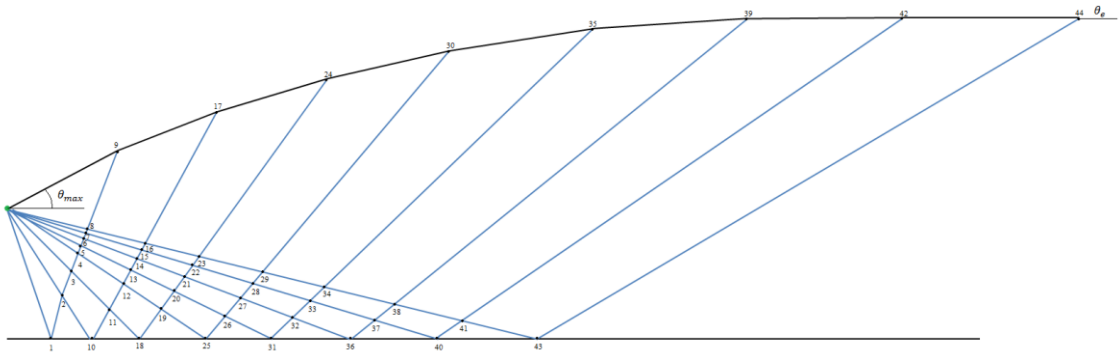

(Figure 17.1) – Mapping of the solutions along a 2D MOC characteristic net for 8 characteristic lines

Since all last points on each characteristic line in the characteristic net (point 8, 16, 23, 29 etc.) cannot change their flow angle from there-on due to the previously defined compatibility equations the following statement is true:

$$\theta_{43} - \nu_{43} = \theta_{44\,(e)} - \nu_{44\,(e)} \tag{71}$$

Due to the perfect expansion assumption made in the "Chemical Kinetics" section of this report, the exhaust velocity should have an axial component only ($v = 0$). This indicates that the velocity vector is horizontal and that $\theta_{44\,(e)} = 0$:

$$\nu_{43} = \nu_{44} \tag{72}$$

The exhaust Mach number was previously said to be a driving parameter. Using the Prandtl-Meyer function the exhaust Prandtl-Meyer angle (ν_{44}) can be numerically extrapolated. For the parameters previously presented:

$$\nu(3.2554) = 72.035° \tag{73}$$

For that Mach number and the known θ_{43} the compatibility constant along that characteristic line for all points is:

$$\theta_{43} + \nu_{43} = K_{-43} = 72.035° \tag{74}$$

Examining figure 17.1 shows that the point at the throat, point 43 and 44 lie on the same set of characteristic lines therefore from equations (73) and (74):

$$\theta_{max} + \nu_{throat} = K_{-43} \tag{75}$$

The expansion at the throat is a Prandtl-Meyer expansion therefore:

$$\theta_{max} = \frac{1}{2}(K_{-_{43}}) \tag{76}$$

Or:

$$\theta_{max} = \frac{\nu(M_e)}{2} = \frac{\nu(3.2554)}{2} = 36.0175\,^\circ \tag{77}$$

At this stage a dilemma with one boundary condition arises. Since nozzles are choked and the fluid is sonic at the throat the undefined expression of $\tan(90)$ occurs in the characteristic equation. A workaround for this problem is setting the throat Mach number to slightly larger than 1 or setting the throat vector angle to slightly larger than 0. In this case:

$$\theta_1 = 1.0175\,^\circ \tag{78}$$

The smaller θ_1 is the more accurate the results. Propagation of the calculation downstream is, as mentioned, based on the constant change in the velocity vector angle. This constant change is known as $\Delta\theta$ and is calculated as follows:

$$\Delta\theta = \frac{\theta_{max} - \theta_1}{number\ of\ characteristic\ lines - 1} \tag{79}$$

For the demonstration nozzle the change in that angle is:

$$\Delta\theta = 5^\circ \tag{80}$$

To begin extrapolating the values for the 44 points, attention is called to the compatibility constant along the first left-running characteristic line $(K_+)_{1\sim8}$. At point 8 it is know that the flow direction angle (θ_8) is half the exhaust Prandtl-Meyer angle. Moreover, the Prandtl-Meyer angle at this point is also equal to half the exhaust Prandtl-Meyer angle thus equal to the flow direction angle. The K_+constant along the first characteristic line is then always equal to zero for all 8 points.

$$\theta_{1\sim8} = \nu_{1\sim8} \tag{81}$$

$$K_{+_{1\sim8}} = constant = 0 \tag{82}$$

The remaining variables can be then calculated with the aid of the following equations:

$$\theta = \frac{1}{2}(K_- + K_+) = \nu \tag{83}$$

$$\nu = \frac{1}{2}(K_- - K_+) = \theta \tag{84}$$

$$K_- = \theta + \nu, \qquad K_{-_{1\sim8}} = 2\theta = 2\nu \tag{85}$$

$$K_+ = \theta - \nu, \qquad K_{+_{1\sim8}} = 0 \tag{86}$$

For the remaining characteristic lines it is known that every point, coincident with the x-axis, has a flow direction angle of 0° and every following θ for a point is increased by $\Delta\theta$. Since the right-running compatibility constant (K_+) must always be equal to the Prandtl-Meyer angle at the wall of the nozzle and it changes with a constant step of $2\Delta\theta$, which was established from the first characteristic line, it is possible to calculate all points in the characteristic net.

When discussing θ_{max} it was confirmed that beyond the points running along the last right-running characteristic line, the flow-field does not change direction therefore:

$$\theta_8 = \theta_9 \qquad \theta_{34} = \theta_{35}$$
$$\theta_{16} = \theta_{17} \qquad \theta_{38} = \theta_{39}$$
$$\theta_{23} = \theta_{24} \qquad \theta_{41} = \theta_{42}$$
$$\theta_{29} = \theta_{30} \qquad \theta_{43} = \theta_{44}$$

The slope of the wall between two wall-points can therefore be calculated by taking the mean value of their inflection angles:

$$\begin{aligned} 9\sim17 &= \frac{\theta_9 + \theta_{17}}{2} \\ 17\sim24 &= \frac{\theta_{17} + \theta_{24}}{2} \\ 24\sim30 &= \frac{\theta_{24} + \theta_{30}}{2} \\ &(\dots) \end{aligned} \tag{87}$$

Once all 4 variables for each point are known, from the Prandtl-Meyer angle the Mach number is approximated numerically and the Mach angle is calculated form the Mach number. Recall that the slope of the characteristic lines is equal to the sum of the inflection angle and Mach angle. The nozzle can then be plotted graphically which for small numbers of characteristic lines is suitable.

Implementation

Since 2D MOC is not used for the final design of the nozzle, developing an automated, software-driven calculation is considered unnecessary for this report. The calculation was semi-automatically

implemented into an MS Excel Spreadsheet with one Macro written in Visual Basic Applications (VBA). The defined function is the numerical extrapolation of the Prandtl-Meyer function since it cannot be rearrange analytically (Figure 20.1).

```
'Kyril Palaveev 2020, SeekerLoopFunction

Function vtom(v, Optional gamma As Variant)

If v = 0 Then Let vtom = 1: Exit Function

If IsMissing(gamma) Then Let gamma = 1.4

For m = 1 To 5 Step 0.00001

    x = (Sqr((gamma + 1) / (gamma - 1))) * (Atn(Sqr((gamma - 1) * (m ^ 2 - 1) / (gamma + 1)))) - (Atn(Sqr(m ^ 2 -
    If x >= v Then Let vtom = m: Exit Function


Next m

End Function
```

(Figure 20.1) – A numerical procedure for calculating Mach number for given Prandtl-Meyer angles in Visual Basic Applications

Once the slopes of the characteristic lines are obtained the Solidworks CAD Software is used to graphically derive the nozzle contour. If the reader decides to explore an automatic implementation of 2D MOC, coordinates for each point can be derived through trigonometry. Triangulating between three points by knowing their slopes is an elementary process. This would allow the user to use 2D MOC to produce nozzle contours with higher accuracy.

Results

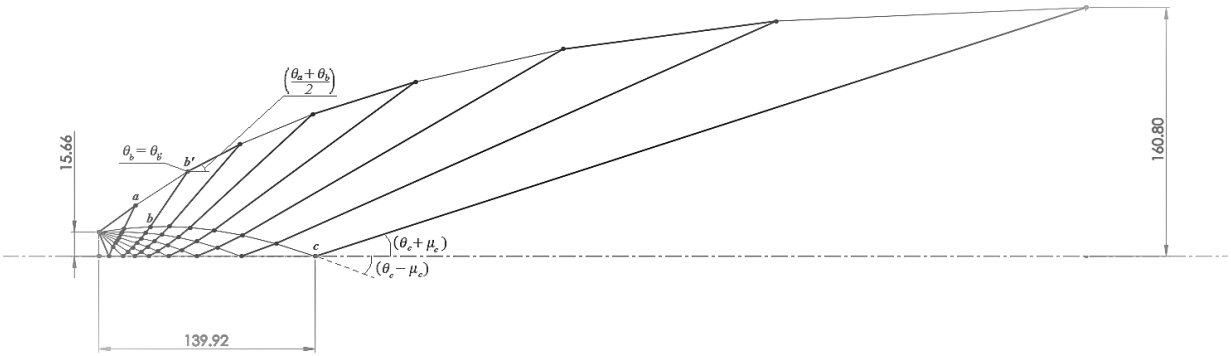

(Figure 21.1) – Graphical Results of 2D MOC for a C-D nozzle with an exhaust Mach number of 3.2554 and 8 characteristic lines

Discussion

When discussing the mathematics behind 2D MOC some of the issues were outlined. Proof from the results section shows that the exhaust nozzle radius is 99.97% larger than the radius calculated using

isentropic theory. The main reason for this error is that the compatibility equation is detached from the area-Mach number relationship. Even though none of the MOC procedures are somehow connected to that relationship more advanced procedures of MOC are iterable, allowing the exhaust area to be adjusted. 2D MOC progresses downstream with some seemingly arbitrary constant which is controlled only by the number of characteristic lines and the exhaust Mach number and is in no way "adjustable" or iterable making it unsuitable for the design of nozzles that are required to reduce the pressure of the flow in a controlled manner so that the exhaust pressure is some desired value. Given that 2D MOC is dimensionless and no additional inputs are required (such as pressure distributions and temperatures) this solution of the partial differential equations is irrelevant and not beneficial when designing nozzle contours. An experimental nozzle with the same number of Mach lines but with a lower Mach number of 2.688 was also made to assess the progression of the error. It is found that the error between the isentropic exhaust radius and the 2D-MOC-obtained exhaust radius decreases to a value of 50.39%. In Anderson's book – "Modern Compressible Flow with Historical Perspective" a 2D MOC nozzle with 7 characteristic lines and an exhaust Mach number of 2.4 is designed. Through approximate measurements it is discovered that that nozzle has an area ratio of 5.0625. For a Mach number of 2.4 however, isentropic theory indicates that the area ratio should in fact be between 3.01 and 2.403 for specific heat ratios between 1.2 and 1.4. The error for Anderson's 2D MOC nozzle is therefore between 22.89 and 31.1%. An interesting discovery is that with a decrease of exhaust Mach number, the error between the isentropic and 2D MOC exhaust radii decreases. Nevertheless the conclusion is that 2D MOC is unsuitable for designing nozzles which are expected to comply with isentropic theory. The method also does not allow for any means to alter the generated error in a meaningful and controlled way.

Axisymmetric Method of Characteristics: Derivation

The general principle of Axisymmetric MOC is identical to that of 2D MOC. The difference arises from the coordinate system in which Axisymmetric MOC lies. The previously defined Cartesian system is replaced by a cylindrical coordinate system:

$$r(v), \qquad \phi(w), \qquad x(u) \tag{88}$$

To better present the change in coordinate system, the following expressions equate each of the cylindrical components to the Cartesian:

$$r = \sqrt{x_{Cart}^2 + y^2} \tag{89}$$

$$\phi = \tan^{-1}\left(\frac{y}{x_{Cart}}\right) \tag{90}$$

$$x = z \tag{91}$$

Note: caution is advised when working with cylindrical coordinates as they may mislead the reader if compared to Cartesian coordinates.

Irrotationality

For this setup irrotational flow is expressed as:

$$\nabla \times \underline{V} = \frac{1}{r}\begin{vmatrix} \hat{l} & r\hat{m} & \hat{n} \\ \frac{\partial}{\partial r} & \frac{\partial}{\partial \phi} & \frac{\partial}{\partial x} \\ v & rw & u \end{vmatrix} = 0 \tag{92}$$

It is evident from equation (92) that the unit vectors are different compared to the Cartesian coordinate system. The unit vectors for a cylindrical coordinate system change with location therefore popularly classified as a local type coordinate system.

Cramer's rule to solve equation (92) indicates that:

$$\frac{\partial u}{\partial r} = \frac{\partial v}{\partial x} \tag{93}$$

Momentum Equation

Recall the Momentum equation:

$$dp = \rho \underline{V} dV = -\frac{\rho d}{2}(u^2 + v^2 + w^2) \tag{94}$$

Due to the type of symmetry of the nozzle the w term is voided.

$$d\rho = -\frac{\rho}{a^2}(udu + vdv) \tag{95}$$

where:

$a^2 = \frac{dp}{d\rho}$

From equation (95) for each spatial term:

$$\frac{\partial}{\partial x}\rho = -\frac{\rho}{a^2}\left(u\frac{\partial u}{\partial x} + v\frac{\partial v}{\partial x}\right) \tag{96}$$

$$\frac{\partial}{\partial r}\rho = -\frac{\rho}{a^2}\left(u\frac{\partial u}{\partial r} + v\frac{\partial v}{\partial r}\right) \tag{97}$$

Continuity Equation

Returning to the Continuity equation:

$$\nabla \cdot \rho \underline{V} = 0 \tag{98}$$

$$\frac{\partial}{\partial x}(\rho u) + \frac{\partial}{\partial r}(\rho v) + \frac{\partial}{\partial \phi}(\rho w) + \frac{\rho v}{r} = 0 \tag{99}$$

Again due to the type of symmetry of the nozzle the ϕ term is voided.

$$\frac{\partial}{\partial x}(\rho u) + \frac{\partial}{\partial r}(\rho v) + \frac{\rho v}{r} = 0 \tag{100}$$

Axisymmetric Method of Characteristics

Characteristic Equation

Substituting the Momentum equation terms ((96) & (97)) into the Continuity equation – equation (100) – yields:

$$\frac{\partial u}{\partial x}\left(-\frac{\rho}{a^2}\left(u\frac{\partial u}{\partial x} + v\frac{\partial v}{\partial x}\right)\right) + \frac{\partial v}{\partial r}\left(-\frac{\rho}{a^2}\left(u\frac{\partial u}{\partial r} + v\frac{\partial v}{\partial r}\right)\right) + \frac{\rho v}{r} = 0 \tag{101}$$

From the velocity potential equation which remains the same as in 2D MOC equation (101) reduces to:

$$\left(1 - \frac{u^2}{a^2}\right)\frac{\partial u}{\partial x} - \frac{vu}{a^2}\frac{\partial v}{\partial x} - \frac{vu}{a^2}\frac{\partial u}{\partial r} + \left(1 - \frac{v^2}{a^2}\right)\frac{\partial v}{\partial r} = -\frac{v}{r} \tag{102}$$

The irrotationality condition gave equation (93) which is now substituted into equation (102):

$$\left(1 - \frac{u^2}{a^2}\right)\frac{\partial u}{\partial x} - 2\frac{vu}{a^2}\frac{\partial v}{\partial x} + \left(1 - \frac{v^2}{a^2}\right)\frac{\partial v}{\partial r} = -\frac{v}{r} \tag{103}$$

The derivatives are then:

$$du = \frac{\partial u}{\partial x}dx + \frac{\partial u}{\partial r}dr \tag{104}$$

$$du = \frac{\partial u}{\partial x}dx + \frac{\partial v}{\partial x}dr \tag{105}$$

$$dv = \frac{\partial v}{\partial x}dx + \frac{\partial v}{\partial r}dr \tag{106}$$

Similar to the 2D MOC philosophy the three derivatives are solved as two 3 by 3 determinants:

$$\frac{\partial v}{\partial x} = \frac{A}{B} = \frac{\begin{vmatrix} 1-\frac{u^2}{a^2} & 0 & 1-\frac{v^2}{a^2} \\ dx & du & 0 \\ 0 & dv & dy \end{vmatrix}}{\begin{vmatrix} 1-\frac{u^2}{a^2} & -\frac{2uv}{a^2} & 1-\frac{v^2}{a^2} \\ dx & dr & 0 \\ 0 & dx & dr \end{vmatrix}} \tag{107}$$

The condition that A/B must equal $0/0$ to obtain valid results holds. More interestingly determinant B is identical to the 2D MOC dividing determinant with the exception that the y-coordinate is occupied by the r-coordinate. This indicates that the slope of the characteristic lines is again governed by the sum or difference of the flow angle and Mach angle. The characteristic equation for Axisymmetric MOC is then:

$$\left(\frac{dr}{dx}\right)_{\boldsymbol{char}} = \frac{-\frac{uv}{a^2} \mp \sqrt{\left(\frac{u^2+v^2}{a^2}\right)-1}}{1-\frac{u^2}{a^2}} \tag{108}$$

Or:

$$\left(\frac{dr}{dx}\right)_{\boldsymbol{char}} = \tan(\theta \mp \mu) \tag{109}$$

Compatibility Equation

For determinant A equal to 0:

$$\frac{dv}{du} = -\frac{\left(1-\frac{u^2}{a^2}\right)-\frac{v}{r}\frac{dr}{du}}{\left(1-\frac{v^2}{a^2}\right)\left(\frac{dr}{dx}\right)_{char}} \tag{110}$$

Equation (110) can also be written in the form:

$$\frac{dv}{du} = -\frac{\left(1-\frac{u^2}{a^2}\right)}{\left(1-\frac{v^2}{a^2}\right)}\left(\frac{dr}{dx}\right)_{char} - \frac{\frac{v}{r}\frac{dr}{du}}{\left(1-\frac{v^2}{a^2}\right)} \tag{111}$$

Substituting the characteristic equation (equation (109)) into equation (111):

$$\frac{dv}{du} = -\frac{\left(1-\frac{u^2}{a^2}\right)}{\left(1-\frac{v^2}{a^2}\right)}\left(\frac{-\frac{uv}{a^2} \mp \sqrt{\left(\frac{u^2+v^2}{a^2}\right)-1}}{1-\frac{u^2}{a^2}}\right) - \frac{\frac{v}{r}\frac{dr}{du}}{\left(1-\frac{v^2}{a^2}\right)} \tag{112}$$

Knowing that the resultant vector is the products of the corresponding trigonometric function of the flow angle and the velocity components and that the Mach number ratio equation (112) reduces to the differential form of the axisymmetric compatibility equation:

$$d\theta = \mp\sqrt{M^2-1}\frac{dV}{V} \mp \frac{1}{\sqrt{M^2-1} \mp cotg(\theta)}\frac{dr}{r} \tag{113}$$

In addition to the Prandtl-Meyer flow equation, equation (113) also describes the change in flow angle relative to the radial location of the vector. Moreover due to the Prandtl-Meyer flow equation, equation (113) can also be written as:

$$d(\theta+\nu) = \frac{1}{\sqrt{M^2-1} \mp cotg(\theta)}\frac{dr}{r} \tag{114}$$

$$d(\theta-\nu) = -\frac{1}{\sqrt{M^2-1} \mp cotg(\theta)}\frac{dr}{r} \tag{115}$$

Methodology

The goal of this section is to reduce the differential equations to sets of algebraic equations which are easily solvable compared to the PDEs. The characteristics equation is solved algebraically as a system of two equations.

Note: All algebraic equations are demonstrated for points 1, 2, and 10 from figure 17.1.

$$\begin{cases} \frac{r_2-r_1}{x_2-x_1} = \tan(\theta_1+\mu_1) \\ \frac{r_2-r_{10}}{x_2-x_{10}} = \tan(\theta_{10}-\mu_{10}) \end{cases} \tag{116}$$

Solving the system for x and r:

$$\therefore x_2 = \frac{r_1 - r_{10} + x_{10}\tan(\theta_{10} - \mu_{10}) - x_1\tan(\theta_1 + \mu_1)}{\tan(\theta_{10} - \mu_{10}) - \tan(\theta_1 + \mu_1)} \tag{117}$$

$$\therefore r_2 = r_1 + (x_2 - x_1)\tan(\theta_1 + \mu_1) \tag{118}$$

The compatibility differential equation is solved using forward finite differencing to reduce it to an algebraic equation (Note: from here-on, V denotes scalar velocity, not a velocity vector):

$$0 = \frac{V_{10} - V_1}{V_1} - (\theta_{10} - \theta_1)\tan(\mu_1) - \frac{\tan(\mu_1)\sin(\mu_1)\sin(\theta_1)(x_{10} - x_1)}{\cos(\theta_1 + \mu_1)r_1} \tag{119}$$

$$0 = \frac{V_{10} - V_2}{V_2} - (\theta_{10} - \theta_2)\tan(\mu_2) - \frac{\tan(\mu_2)\sin(\mu_2)\sin(\theta_2)(x_{10} - x_2)}{\cos(\theta_2 + \mu_2)r_2} \tag{120}$$

Equations (119) and (120) are rearranged in terms of the velocity – V and flow angle – θ.

$$V_2 = \frac{1}{\frac{cotg(\mu_1)}{V_1} + \frac{cotg(\mu_{10})}{V_{10}}}[cotg(\mu_1)(1 + \mathbb{P}_1(x_2 - x_1)) + cotg(\mu_{10})(1 + \mathbb{Q}_{10}(x_2 - x_{10})) + \theta_{10} - \theta_1] \tag{121}$$

$$\theta_2 = \theta_1 + cotg(\mu_1)\left(\frac{V_2 - V_1}{V_1}\right) - \mathbb{P}_1(x_2 - x_1) \tag{122}$$

where:

$$\mathbb{P}_1 = \frac{\tan(\mu_1)\sin(\mu_1)\sin(\theta_1)}{r_1\cos(\theta_1 + \mu_1)}$$

$$\mathbb{Q}_{10} = \frac{\tan(\mu_{10})\sin(\mu_{10})\sin(\theta_{10})}{r_{10}\cos(\theta_{10} - \mu_{10})}$$

One specific case however, cannot be solved with equations (121) and (122). That case is when the two points from which the third is solved are on the centerline (such as 2 and 10). Since they have a radial coordinate of 0 and a flow direction of 0, a division by zero is created. Shapiro (1954) demonstrated a solution to this problem[11] by taking the limiting form of $\mathbb{P}_1$ & $\mathbb{Q}_{10}$:

$$\lim_{\substack{r_1 \to 0 \\ \theta_1 \to 0}} \mathbb{P}_1 = \lim_{\substack{r_1 \to 0 \\ \theta_1 \to 0}} \frac{\tan(\mu_1)\sin(\mu_1)\sin(\theta_1)}{r_1\cos(\theta_1 + \mu_1)} \tag{123}$$

$$\lim_{\substack{r_{10}\to 0\\ \theta_{10}\to 0}} \mathbb{Q}_{10} = \lim_{\substack{r_{10}\to 0\\ \theta_{10}\to 0}} \frac{\tan(\mu_{10})\sin(\mu_{10})\sin(\theta_{10})}{r_{10}\cos(\theta_{10}-\mu_{10})} \tag{124}$$

Equations (123) and (124) reduce to:

$$\lim_{\substack{r_1\to 0\\ \theta_1\to 0}} \mathbb{P}_1 \cong \frac{\theta_3}{r_3} \tag{125}$$

$$\lim_{\substack{r_{10}\to 0\\ \theta_{10}\to 0}} \mathbb{Q}_{10} \cong \frac{\theta_3}{r_3} \tag{126}$$

At this stage, the above equations are sufficient to provide a vector's position, flow angle, and velocity. To find the Mach angle for the next point along the characteristic net, the Mach number is needed. The temperature at that point can therefore be calculated using:

$$T_2 = T_c - \frac{V_2^2}{2c_p} \tag{127}$$

The Mach number is therefore:

$$M_2 = \frac{V_2}{\sqrt{\gamma R T_2}} \tag{128}$$

And finally the Mach angle:

$$\mu_2 = \operatorname{asin}\left(\frac{1}{M_2}\right) \tag{129}$$

Recall that the compatibility equations were solved with a first order accurate forward difference. The typical engineering grade accuracy for any differential equation is second order accurate. In need to increase the accuracy of the results, an iterative procedure is introduced which consists of the exact same algebraic equations but with the mean values of the slopes between points 1~2 and 10~2.

Second iteration for the x-coordinate:

$$x_2^{ii} = \frac{r_1 - r_{10} + \left(\frac{\tan(\theta_{10}-\mu_{10})+\tan(\theta_2-\mu_2)}{2}\right)x_{10} - \left(\frac{\tan(\theta_1+\mu_1)+\tan(\theta_2+\mu_2)}{2}\right)x_1}{\left(\frac{\tan(\theta_{10}-\mu_{10})-\tan(\theta_1+\mu_1)+\tan(\theta_2-\mu_2)-\tan(\theta_2+\mu_2)}{2}\right)} \tag{130}$$

Second iteration for the radial coordinate:

$$r_2^{ii} = r_1 + (x_2 - x_1)\left(\frac{\tan(\theta_1 + \mu_1) + \tan(\theta_2 + \mu_2)}{2}\right) \tag{131}$$

Second iteration for the velocity:

$$V_2^{ii} = \frac{\mathbb{N} + \mathbb{C} - \theta_1 + \theta_{10}}{4((V_1 + V_2)^{-1}(\tan(\mu_1) + \tan(\mu_2))^{-1} + (V_{10} + V_2)^{-1}(\tan(\mu_{10}) + \tan(\mu_2))^{-1})} \tag{132}$$

where:

$$\mathbb{N} = \frac{2}{\tan(\mu_1) + \tan(\mu_2)}\left[\frac{2V_1}{V_1 + V_2} + \frac{\mathbb{P}_1 + \mathbb{P}_2}{2}(x_2 - x_1)\right]$$

$$\mathbb{C} = \frac{2}{\tan(\mu_{10}) + \tan(\mu_2)}\left[\frac{2V_{10}}{V_{10} + V_2} + \frac{\mathbb{Q}_{10} + \mathbb{Q}_2}{2}(x_2 - x_{10})\right]$$

Second iteration for the flow angle:

$$\theta_2^{ii} = \theta_1 + \frac{2}{\tan(\mu_1) + \tan(\mu_2)}\left(\frac{2(V_2^{ii} - V_1)}{V_2^{ii} + V_1} - \frac{\mathbb{P}_1 + \mathbb{P}_2}{2}(x_2 - x_1)\right) \tag{133}$$

Once the second iteration is complete, the values from that calculation are treated as the values that would continue the calculation along the net:

$$x_2^{ii} \rightarrow x_2$$

$$r_2^{ii} \rightarrow r_2$$

$$V_2^{ii} \rightarrow V_2$$

$$\theta_2^{ii} \rightarrow \theta_2$$

The iterative process can be repeated multiple times and to determine a suitable iteration count a convergence study is conducted by measuring the exhaust radius of the nozzle for some constant and arbitrary inputs and a varying iteration count (Graph 29.1).

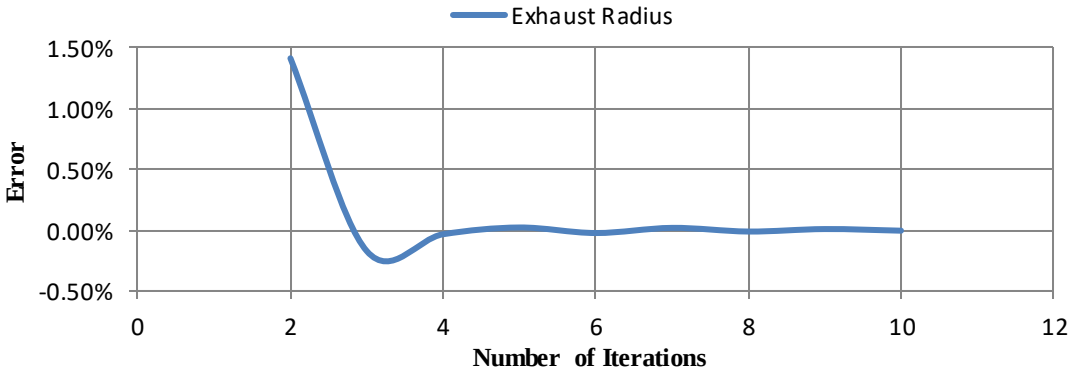

(Graph 29.1) – Convergence study for iteration count of Axisymmetric MOC

Graph 29.1 indicates that after the 5th iteration, the error – difference in exhaust diameter for some arbitrary and constant inputs and a varying iteration count – oscillates between 0.02 and -0.02% which is a reasonable accuracy for a theoretical nozzle design. With a further increase in iterations, the oscillations dampen and the error reduces even further.

To finalize the Axisymmetric MOC procedure the wall points and nozzle contour slopes must be found. From planar MOC, the assumption that the flow does not accelerate or change direction between the last point in the characteristic net and the wall can be used. The inclination or slope of the wall contour segments, as in 2D MOC, is the average between the flow direction of the previous wall point and the flow direction of the last point of the net on the characteristic line on which the calculated wall point lies (e.g. the slope for line 17~24 is the average of θ_9 & θ_{16}). We can therefore write the following equations based on the formulae for the intersection of two lines:

$$x_{17} = \frac{-x_{16}\tan(\theta_{16} + \mu_{16}) + r_{16} + x_9 \tan\left(\frac{\theta_T + \theta_8}{2}\right) - r_8}{\tan\left(\frac{\theta_T + \theta_8}{2}\right) - \tan(\theta_{16} + \mu_{16})} \tag{134}$$

$$r_{17} = \tan(\theta_{16} + \mu_{16})(x_{17} - x_{16}) + r_{16} \tag{135}$$

The number of boundary conditions for Axisymmetric MOC is larger than that of 2D MOC. The variability in these boundary conditions is also greater. The first and most obvious is the initial expansion angle which for 2D MOC was derived to be half the exhaust Prandtl-Meyer angle. No such equation exists in the world of Axisymmetric MOC therefore the initial expansion angle can theoretically be any value between 0 and 90 degrees. This parameter heavily influences the exhaust radius and its selection is based on complicated concepts which are later discussed.

With this procedure, no information is given about any point. Furthermore recall that the algebraic equation examples initiated from points 1 and 10 to calculate point 2. This implies that an important boundary is the axis of symmetry or more specifically – the points that lie on the x-axis (Figure 30.1).

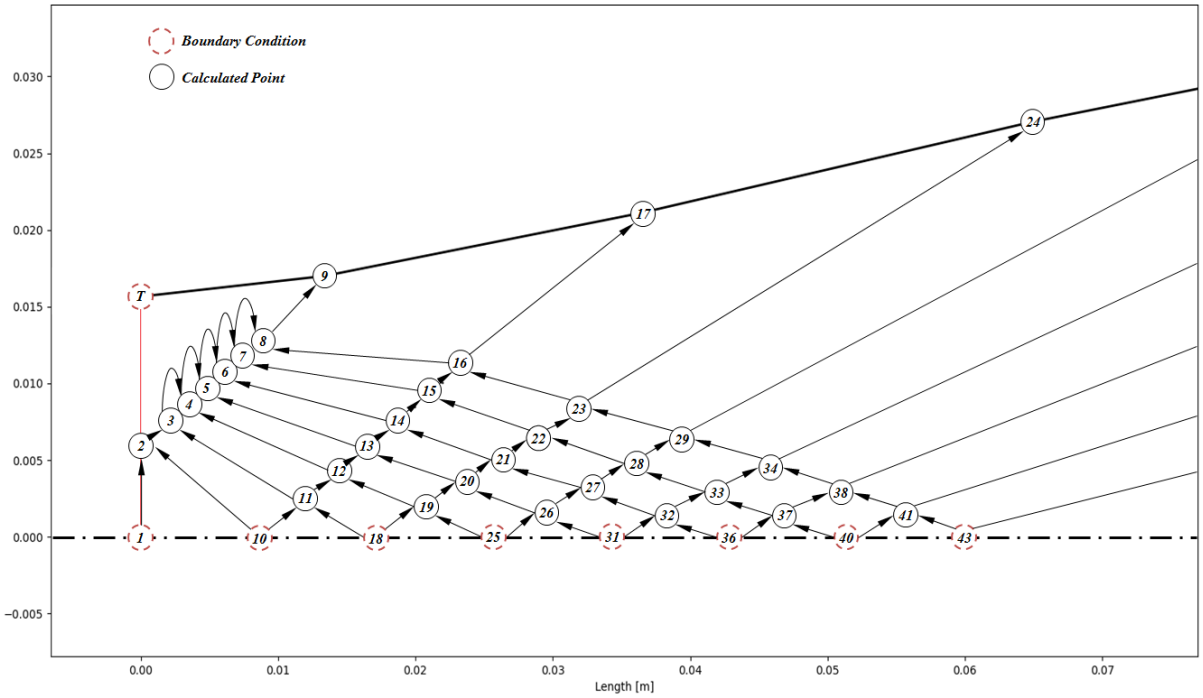

(Figure 30.1) – A flow chart of the Axisymmetric MOC numerical procedure

The most important step for initializing Axisymmetric MOC is calculating the gas properties and position of the points on the x-axis. An obvious parameter is that these point have a radial coordinate of 0. The spacing between each of the points is considered constant and a distribution length is selected (distance from point 1 to 43). Usually the *characteristic net length* is larger than the isentropic throat radius. Now the spatially defined points require an input of information that would yield gas properties at those locations. Specifying the change in pressure as a function of the characteristic net length is ideal. From the known pressure at each point and the known exhaust pressure, the Mach number is calculated and therefore all other properties can also be calculated. The pressure distribution can be either theoretical or experimental. Due to the lack of any experimental data, the theoretical approach is chosen. Suitable for supersonic flows are two types of pressure distributions. The parabolic and cubic pressure distribution functions are both functions of axial distance. The difference is that the cubic distribution is more configurable due to a dimensionless factor known as the q-factor (equations (136) & (137)).

Parabolic pressure distribution[9,10]:

$$\ln(p_x) = L_n^{-2}(x - L_n)^2(\ln(p_t) - \ln(p_e)) + \ln(p_e) \qquad (136)$$

Cubic pressure distribution[9,10]:

$$\ln(p_x) = \left(\frac{qL_n + 2(\ln(p_t) - \ln(p_e))}{L_n^3}\right)x^3 - \left(\frac{2qL_n + 3(\ln(p_t) - \ln(p_e))}{L_n^2}\right)x^2 + qx + \ln(p_t) \quad (137)$$

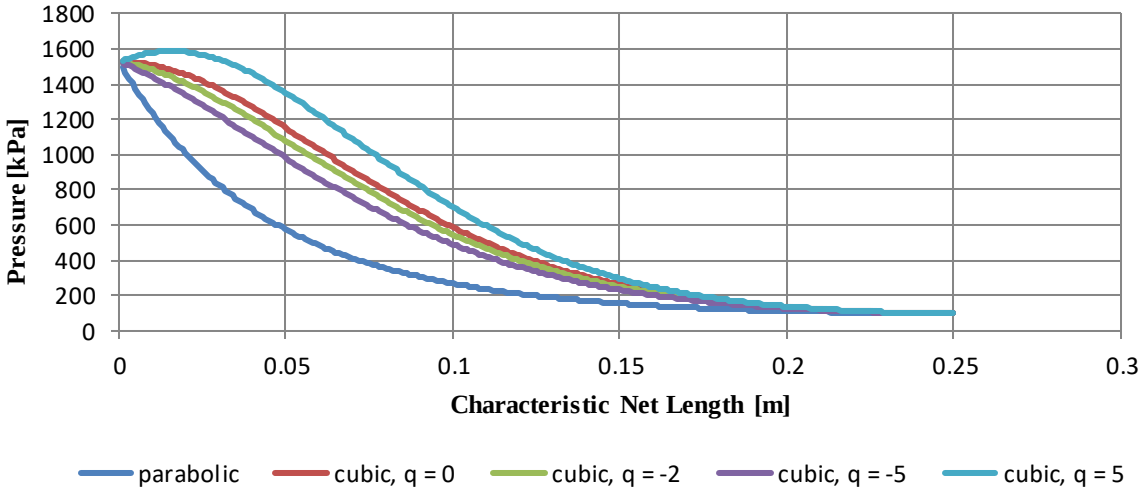

(Graph 31.1) – Graphical representation of equations 136 and 137

It is important to note that extreme q-factor values are not recommended if the distribution is not verified against a distribution that is known to be accurate. Moreover, for a pressure distribution in the supersonic regime, negative q-factors are used.

Results for Low-resolution Nozzle

With the methodology behind the method complete, it is of vital importance that the iterative adjustments of the boundary conditions are outlined. It is known that the isentropic exhaust radius is the radius that the Axisymmetric MOC nozzle exhaust must reach. For the 8-characteristic-lines example, an arbitrary expansion angle of 0.01 [rad] is selected. It is arbitrary since the calculated region with the procedure does not allow for analysis in the transonic region. The pressure distribution type is selected to be parabolic and an initial characteristic net length of 0.1 [m] is selected. The calculation is initiated and for that first iteration, the Axisymmetric MOC exhaust radius calculated to be 0.04296 [m] – 16.3% smaller than the isentropic radius of 0.04996 [m]. At this stage it is recommended to increase the characteristic net length which would explicitly increase the exhaust radius. Through a steady increase in characteristic net length, an error of 0.36% is achieved for a net length of 0.135 [m]. Typically errors below $\pm 1\%$ are considered valid results.

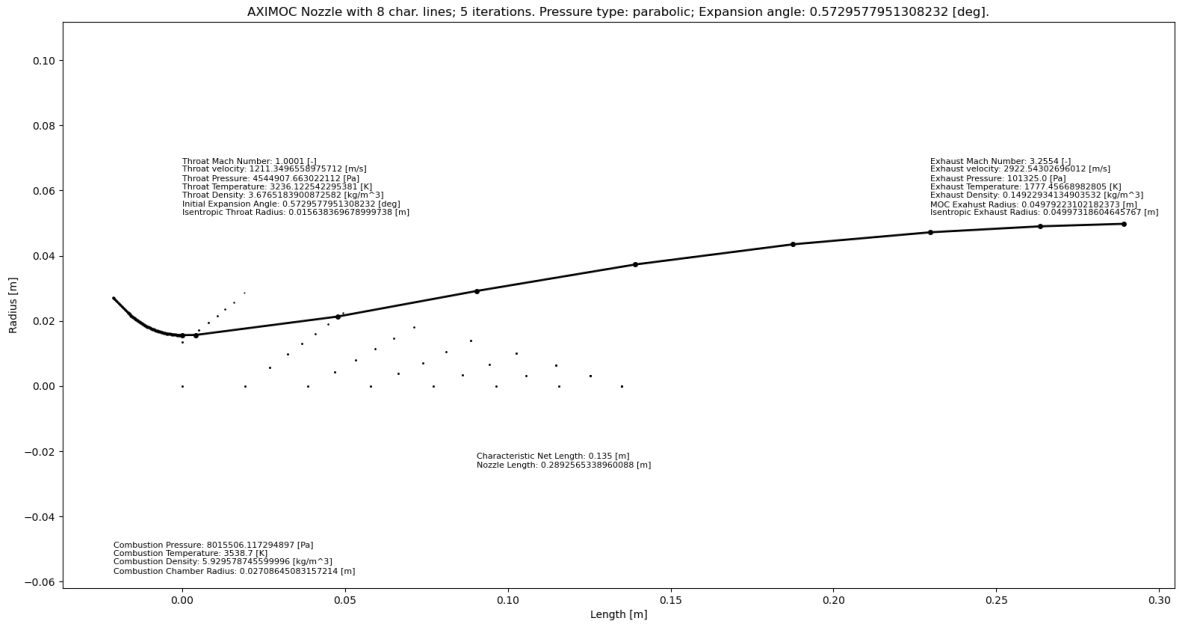

(Graph 32.1) – Nozzle contour generated with Axisymmetric MOC with 8 characteristic lines

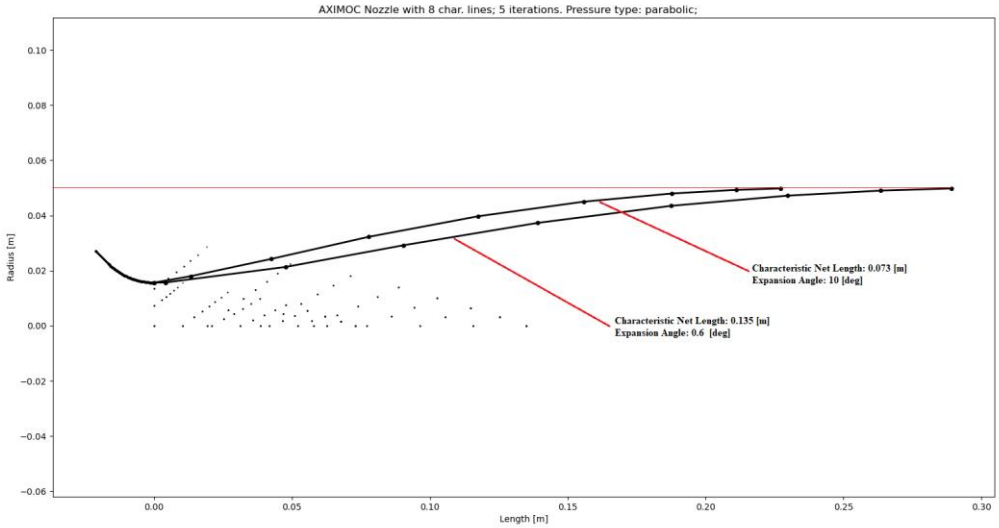

(Graph 32.2) – A graphical demonstration of the influence of the expansion angle on nozzle length

Discussion for Low-resolution Nozzle

Note that the characteristic net crosses the nozzle wall contour. This is actually a common occurrence in nozzles with low initial expansion angles and can still be considered a valid result for this specific procedure. Proof supporting this statement is in Graph 32.2 – two nozzles with identical exhaust radii

but different expansion angles. It is evident that the characteristic net is adjusted to arrive at the same radius. A larger expansion angle requires a shorter net length and vice versa. It is also seen that the larger the expansion angle the shorter the nozzle. In rocketry this is especially desirable as it reduces the weight of the nozzle. However, excessive expansion angles cause geometrical issues. When the nozzle turns into the flow abruptly an oblique shock is produced. An analogy can be made with supersonic flow over a ramp. Other issues include an abrupt separation of the flow which may separate at different times at different radial section of the nozzle which would cause an oscillatory regime. These regimes are especially dangerous in practice as they can lead to structural failures of the nozzle.

It was mentioned that the number of characteristic lines also alter the exhaust radius. The example nozzle with 8 Mach lines is not suitable for a final nozzle contour design. To deduce a suitable number of characteristic lines for a final design a convergence study is presented. The process behind the study is solving a nozzle contour for some constant set of inputs and increasing the number of characteristic lines gradually. The exhaust radius is recorded and the difference between the previous and next calculation is calculated.

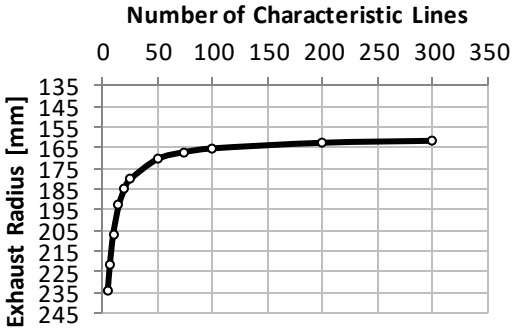

(Graph 33.1) – Number of characteristic lines convergence study measured by exhaust radius.

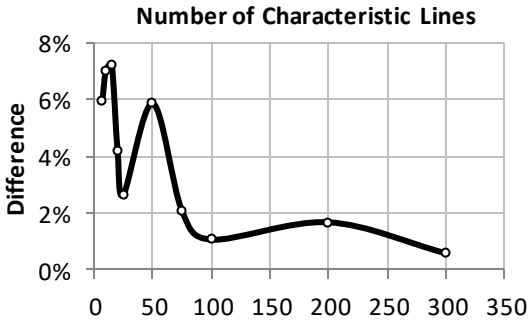

(Graph 33.2) – Number of characteristic lines convergence study measured by percentile error of the difference in exhaust diameter for previous and current number of characteristic lines.

Examining Graphs 33.1 and 33.2 indicates that 200 characteristic lines produce a contour with an error of 1.674%. For this paper it is considered that this error is suitable for an accurate diverging contour thus that nozzle design is produced with 200 characteristic lines.

Results for High-resolution Nozzle

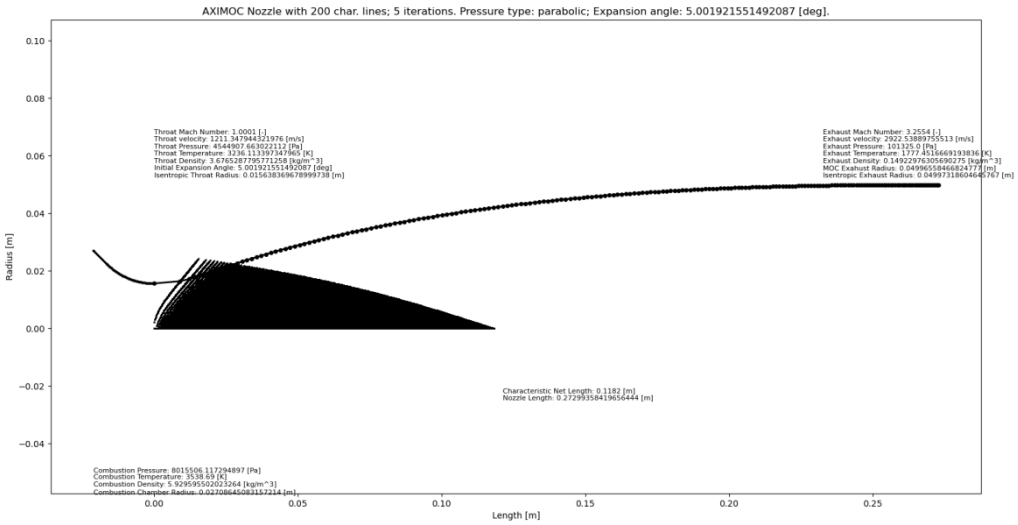

(Graph 34.1) - Nozzle contour generated with Axisymmetric MOC with 200 characteristic lines

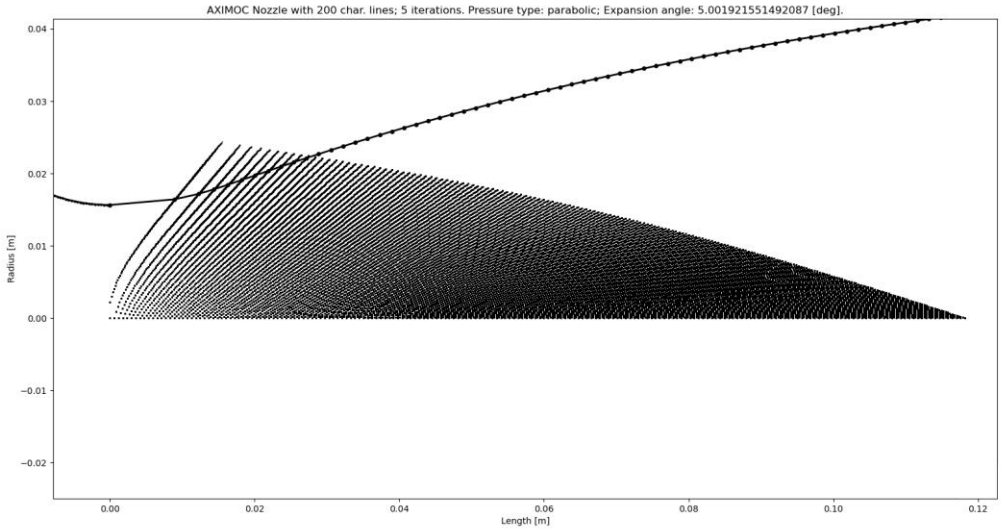

(Graph 34.2) – Close-up on the kernel of an Axisymmetric MOC-generated nozzle with 200 characteristic lines

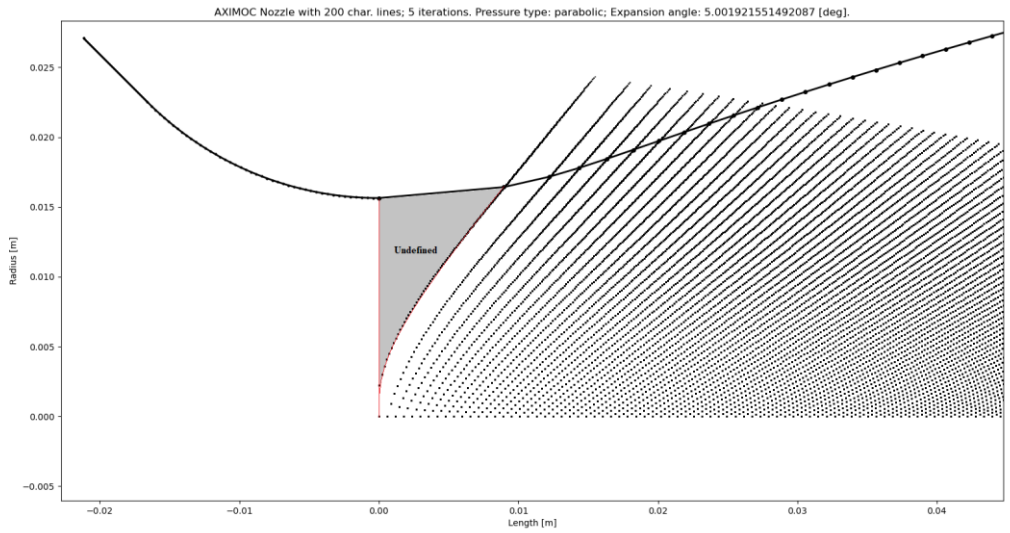

(Graph 35.1) – Close-up of the undefined transonic region in the kernel

Discussion for High-resolution Nozzle

For the chosen parameters shown in Graph 34.1, the produced contour is considered converged with an exhaust radius error minimized to 0.1% when compared to the exhaust radius calculated using isentropic theory. The slightly over-expanded nozzle is with a radius of 0.04996 [m] and the resolution of the contour is generally high with the exception of the transonic region. Graph 35.1 acquaints the reader with a region marked as undefined. This region occurs because of the nature of nozzle flows. Typically, immediately after the throat, the flow changes its properties for a relatively short distance – the flow expands abruptly. Due to this fact, the characteristic lines closer to the throat are curved towards the exhaust significantly more than lines towards the end of the characteristic net. This region can be neglected for nozzles of smaller dimensions but larger nozzles require a fix to ensure that shockwaves and flow separation do not occur. Furthermore the expansion angle of 5 degrees is chosen arbitrarily since at this stage there are no means of calculating a precise expansion angle. Typically expansion angles for contoured nozzles are between 0 and 8 degrees depending on their application. A distinctive for Axisymmetric MOC contour is the length of the nozzle caused by the boundary conditions of the method. In rocketry, nozzles with such high efficiencies are rarely use due to their dimensions and weight.

Implementation

The reader may have suspected that the Axisymmetric MOC procedure is more complicated and labor-intensive than 2D MOC. Therefore the author of this paper developed a computer programme written in Python 3.7. The software consists of equations used to calculate the isentropic relations of the

wanted nozzle followed by the algebraic equations for Axisymmetric MOC. The algorithm is semi-automated at this stage – excluding the automatic adjustment of the characteristic net length. As seen in the results section, only the characteristic line intersections are displayed and this is solely to reduce the usage of graphical and access memory. This is especially useful for large numbers of characteristic lines. The software is intended to be available to the general public as a Windows executable (.exe) and for that reason the author developed a Graphical User Interface (GUI) in order to be more easily used by users.

The "space-marching" procedure of Axisymmetric MOC is achieved in the code by using lists which are indexable and for-loops which call the points' parameters in a specific order based on their index to perform the calculation. All other implementations of various isentropic, thrust, and thermodynamic calculations are trivial since they are not involved in any complicated repetitive loops, lists or conditional statements. To simplify the use of the software a minimum input study was conducted to reduce the number of inputs to a minimum and ensure that non-corresponding inputs cannot be entered. The GUI and inputs of the software are shown in figure 36.1.

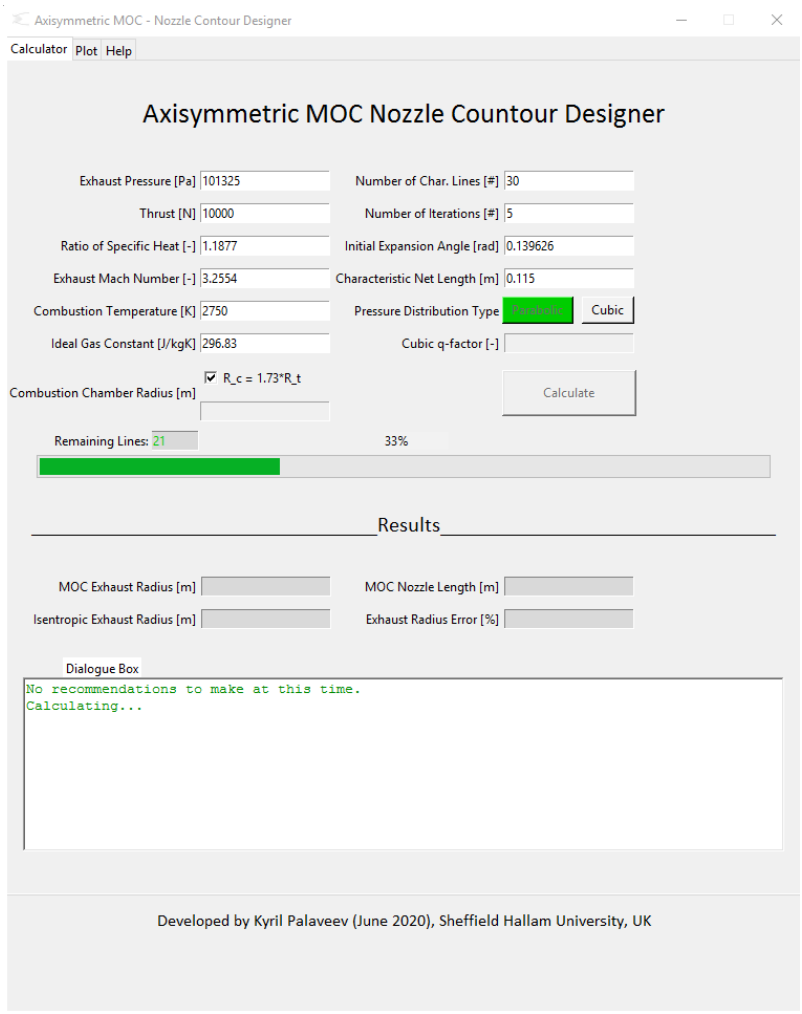

(Figure 36.1) – The Graphical User Interface of the developed Axisymmetric MOC nozzle

contour designer.

Note: Instructions on how one can acquire and setup the software can be found in Appendix A.

Further Considerations

The most important part of Axisymmetric MOC is implemented and a nozzle contour is created. However, further work is required which is classed as outside the scope of this paper to avoid prolonging the paper to a great extent. The characteristic net demonstrated in this paper is known as the *kernel*. The kernel is the most important section of the nozzle design procedure as it constructs the greatest segment of the nozzle contour. A useful feature of Axisymmetric MOC is that for almost any given boundary conditions a characteristic net can be constructed. Such example is the evaluation of the undefined transonic region. Sauer's method[9] can provide a parabolic sonic line at the throat which can then be treated as a characteristic line and a net can be computed between the first kernel characteristic line and the parabolic sonic line. This addition to the nozzle design procedure would allow for a justified selection of the initial expansion angle. For the purposes of this paper the expansion angle is selected based on common expansion angles for rocket nozzles. However, a point where the nozzle is shortest and produces no shocks does exist and this point can be found through the transonic region analysis procedure. A third characteristic net can also be constructed utilizing the top-most layer of the kernel and the undefined region as a boundary condition. This net is referred to as the *boundary* and it can span beyond the nozzle wall contour. The boundary region is used to determine the location of the contour since the introduction of the transonic analysis procedure would discontinue the currently used solution between the expansion nozzle contour and the diverging nozzle contour (Figure 37.1).

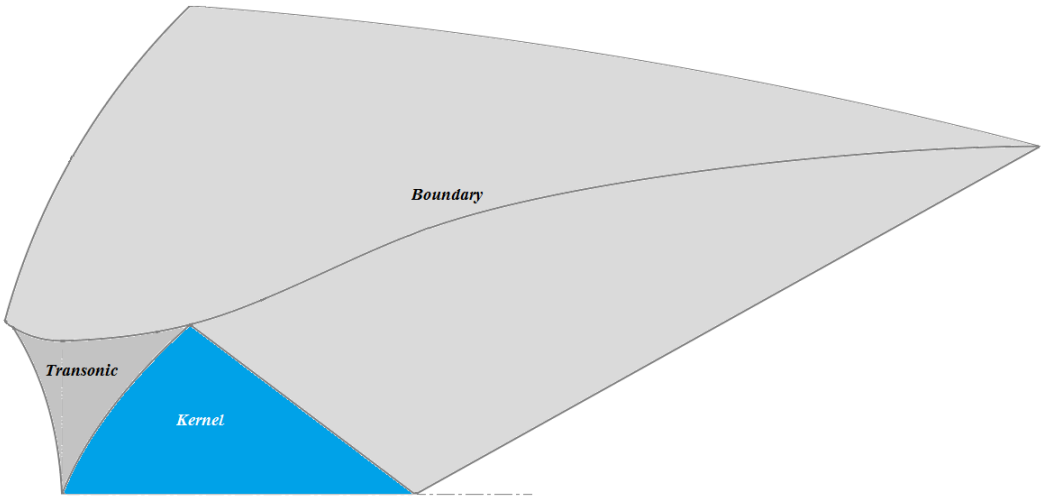

(Figure 37.1) – Different regions of a nozzle that require separate characteristic nets for a refined nozzle geometry

Converging Nozzle

Now that the diverging section is obtained, the converging section must be designed. Due to the flow being in the subsonic regime at that section of the nozzle, its geometry is not as critical. A conical converging section would not satisfy our overall nozzle geometry as a sharp corner would be produced at the throat which would separate the flow. Rao's method[12] is a straightforward technique which utilizes circular arcs. The radii of these arcs have been derived experimentally and have proven to yield satisfactory converging nozzle contours. Typically Rao's converging geometry consists of two tangential circular arcs however, since we are not focusing on the design of the combustion chamber, only one of the circular arcs is used and an additional tangential to that arc line is extended from the end of circular arc to meet the desired combustion chamber radius (Figure 38.1).

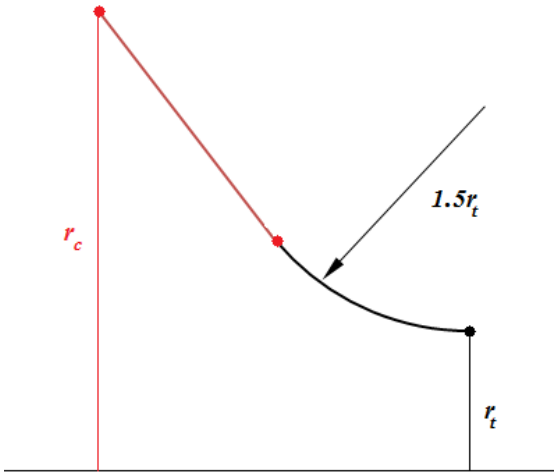

(Figure 38.1) – Converging section with Rao's radius.

The length of the circular arc is typically between 40 and 45 degrees and it can be plotted numerically using the following equations:

$$x = 1.5r_t \cos(\beta) \tag{138}$$

$$r = 1.5r_t \sin(\beta) + 2.5r_t \tag{139}$$

for $-135° < \beta < -90°$

CFD Validation

Despite the need of further refinement of the transonic and boundary region a CFD simulation of the high-resolution nozzle contour is attempted to verify aspects of the nozzle, such as desired exhaust gas

properties. The simulation also acquaints the reader with the behavior of nozzle flows along the axis of symmetry.

Mesh

The generated axisymmetric nozzle contour is imported into the software and a domain is formed. A fluid surface is created and split in multiple sections for ease of meshing.

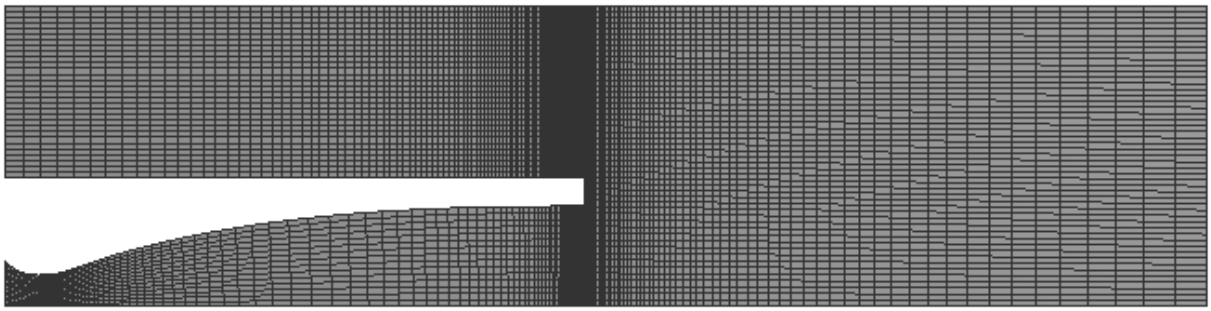

(Figure 39.1) – Generated mesh for the computational domain of a rocket nozzle

The mesh in figure 39.1 has two important bias features one of which is towards the throat of the nozzle and one – towards the exhaust. A finer mesh is required at these locations due to the rapid change of fluid properties and fluid direction. The used mesh for this simulation consists of 7971 nodes and 7650 elements. The quality of the mesh can be examined in table 39.1.

Mesh Metric	**Average Value**
Skewness	1.0984×10^{-2}
Aspect Ratio	2.5564
Orthogonal Quality	0.9985

(Table 39.1) – Mesh quality parameters

Physics Setup

Since the assumptions used to generate the axisymmetric nozzle are inviscid and irrotational flow, the simulation is run with those same assumptions. Nozzle flows however are in many cases oscillatory. In the case of an inviscid nozzle flow simulation, a lack of boundary layer causes a zero-damping condition for the oscillatory flow which causes the simulation to diverge. A solution to this issue is running a transient simulation. Once set, the model is selected to be inviscid with the energy equation. The fluid is defined per the parameters from this report and the newly created fluid is used for the simulation. The boundary conditions are set as seen in figure 40.1 and table 40.1.

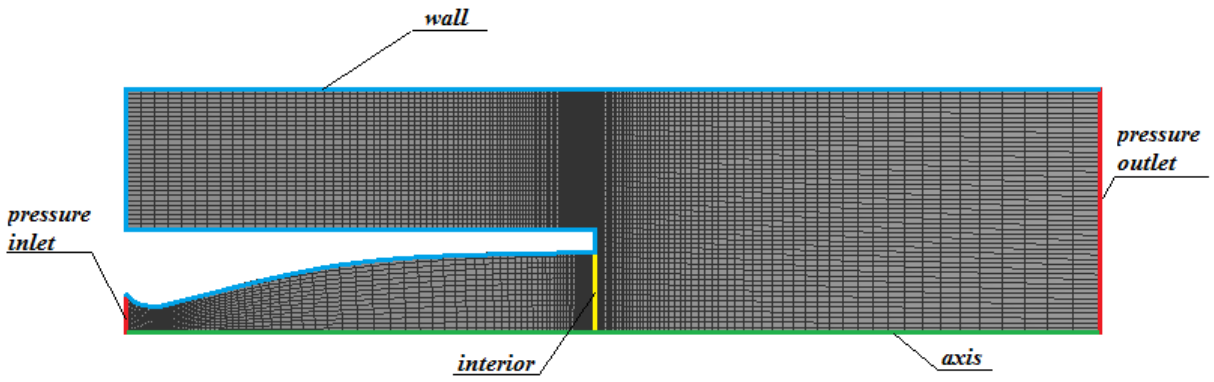

(Figure 40.1) – Location of boundary conditions

Boundary Condition	Input Parameters
Pressure Inlet	8 000 000 $[Pa]$ / 3538.69 $[K]$
Interior	N/A
Axis	N/A
Wall	N/A
Pressure Outlet	101325 $[Pa]$ / 300 $[K]$
Operating Conditions	0 $[Pa]$

(Table 40.1) – Input parameters for all boundary conditions in figure 40.1

The residuals are set to 10^{-6} and additional monitors for the nozzle exhaust are set. The initialization is hybrid and the calculation is initiated with a constant time-step of 1×10^{-5} $[sec]$ and a total of 1100 time-steps. The maximum iteration-count per time-step is set to 1000.

Setup Summary	
General Model	Density-Based
	Transient
	Axisymmetric
Equations	Energy
	Inviscid
Material	Fluid
	Constant Ideal Gas
Reference Value	Inlet
Methods	Flow: Second Order Upwind
	Transient: Second Order Implicit
Residuals	1e-06 [-]
Initialization	Hybrid

Time Advancement	Fixed
	User-Specified
Number of Time Steps	1100
Time Step Size	1e-05 [sec]
Max Iteration per Time Step	1500

(Table 41.1) – Summary of the CFD physics setup for an inviscid rocket nozzle

Convergence Validation

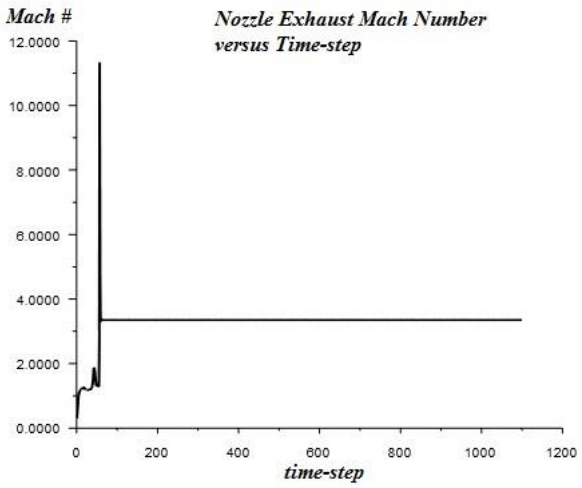

(Graph 41.1) – Exhaust Mach number CFD monitor

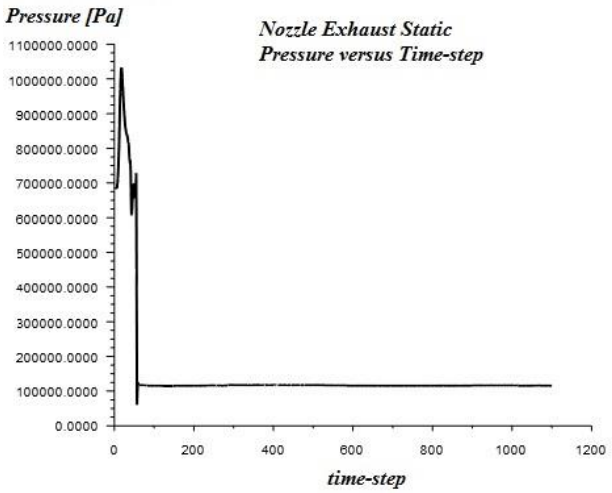

(Graph 41.2) – Exhaust pressure CFD monitor

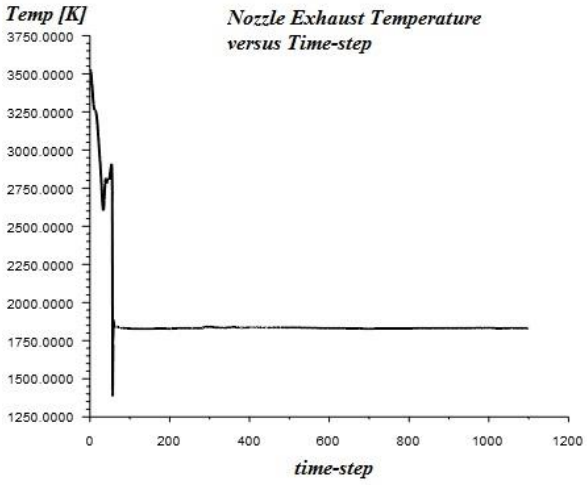

(Graph 41.3) – Exhaust temperature CFD monitor

Graphs 41.1, 41.2, and 41.3 are monitors positioned at the nozzle exhaust. The values at that point are important to obtain via CFD as they are already known through isentropic theory and can be directly compared to judge the validity of the simulation. When compared to the isentropic values, the

monitors indicate that the numerically calculated values are acceptable since all three parameters have an error of less than 1%.

Property at Exhaust	Analytical	Numerical	Error
Mach Number [-]	3.255	3.275	0.614%
Pressure [Pa]	101325	102212	0.875%
Temperature [K]	1 779.96	1767.35	0.708%

(Table 42.1) – Validation of gas properties at exhaust

Results

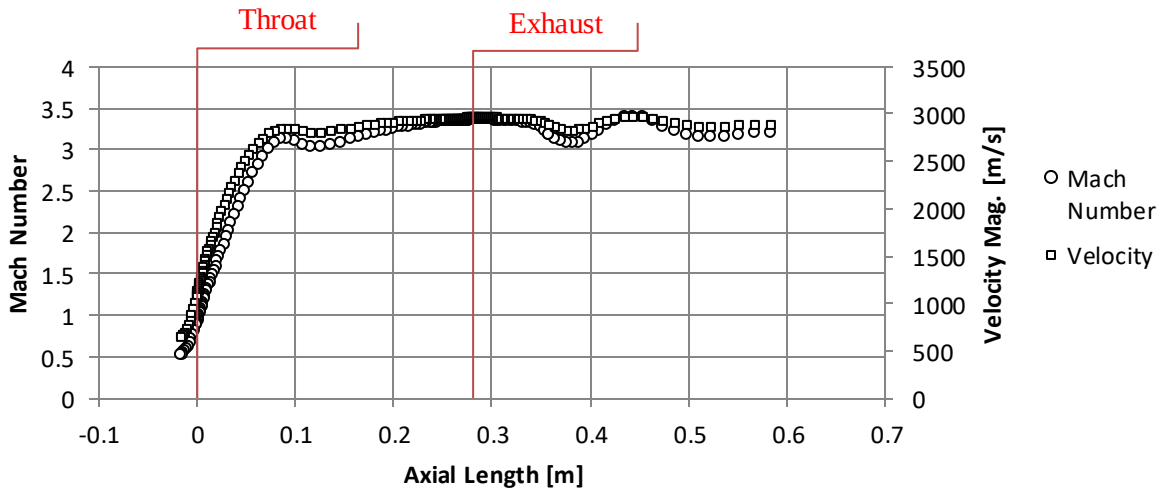

(Graph 42.1) – CFD velocity magnitude and Mach number versus nozzle axis

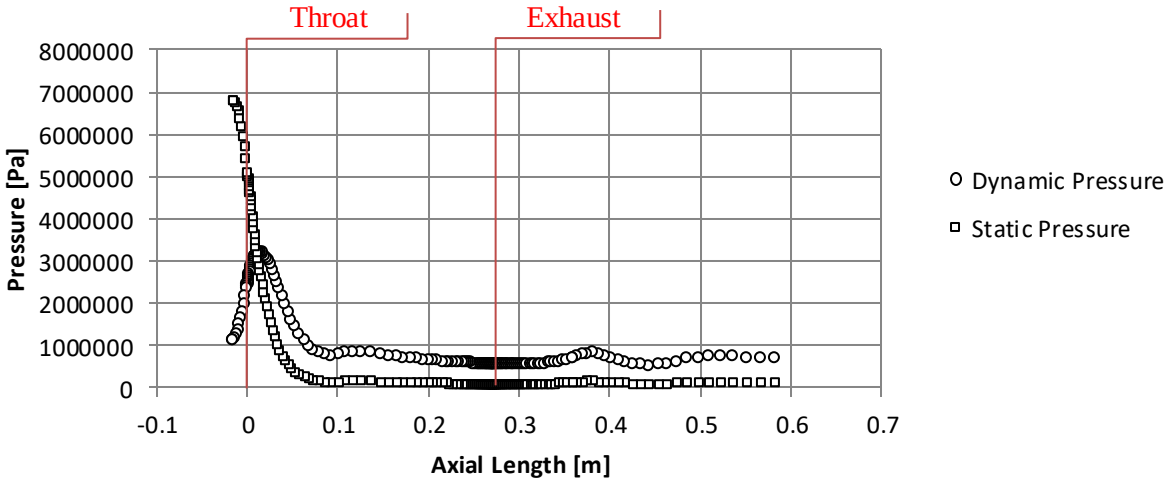

(Graph 42.2) – CFD static and dynamic pressure versus nozzle axis

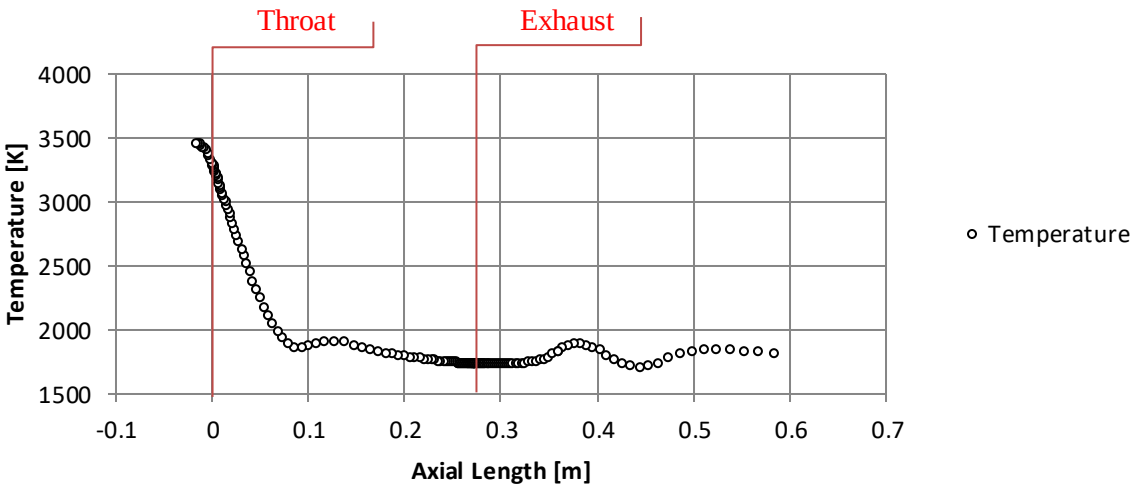

(Graph 43.1) – CFD temperature versus nozzle axis

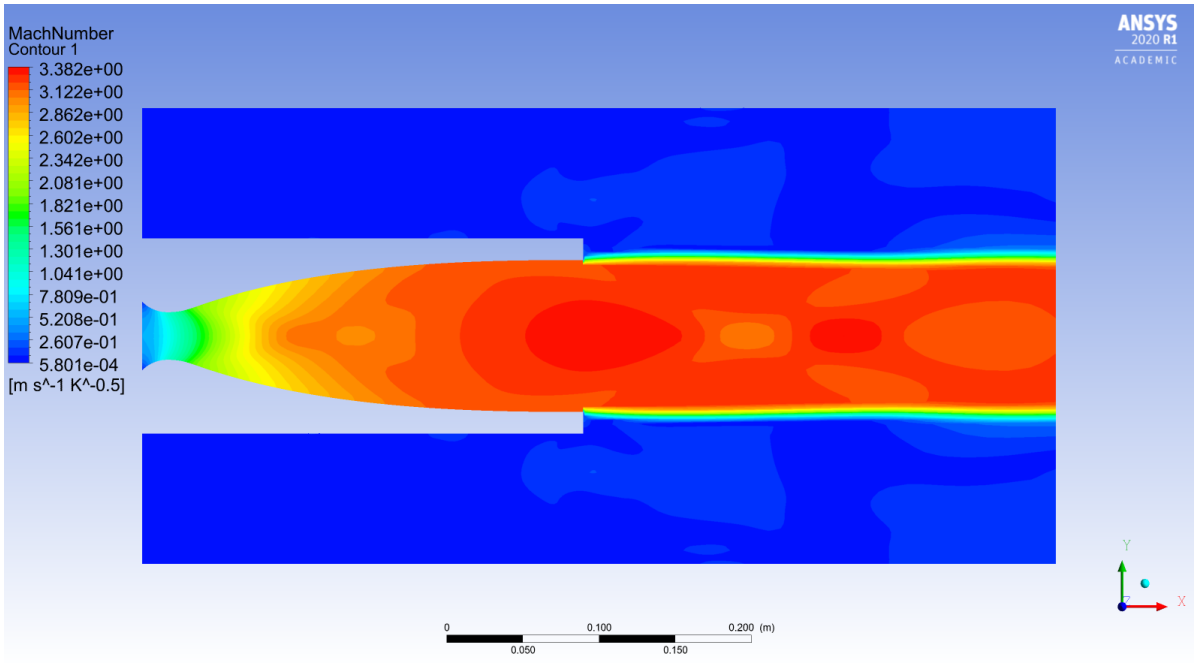

(Figure 43.1) – CFD contour of Mach number

Discussion

Despite the large amount of information that CFD can provide, the presented data is relatively concise in order to focus on examining the general flow properties of the working fluid inside an axisymmetric MOC nozzle. For each of the three graphs, the flow between the converging section and immediately after the throat ($-0.015 < x < 0.07$) the gradient is high. The reader may recall that this rapid change

in properties is due to the rapid expansion for a relatively short distance associated with nozzles. Advancing downwind, at $x = 0.09$ an expected phenomenon is observed. As previously stated the geometry needs further refinement of the transonic and boundary region and the CFD simulation now provides strong evidence to why that is needed. Examining the velocity graph (Graph 42.1), a drop in velocity magnitude of approximately 50 m/s is observed. This indicates the generation of a weak shock. The shock would have been exacerbated if a larger expansion angle was selected thus this simulation being proof that the selected expansion angle is relatively suitable and the generated shock is weak enough to be neglected for this paper. Nevertheless the shock can be minimized even further if the expansion angle is reduced.

Following the shock and up to the exhaust of the nozzle, the graphs show that the rate of change of the properties of the gas decreased by a significant amount. This raises another flaw of MOC and it is associated with mechanically inefficient nozzles. Despite the nozzle being theoretically 100% thermodynamically efficient, in practice the nozzles are longer than desired from a practical stand point. The graphs suggest that it is needn't for the nozzle to exceed such lengths as the properties' rate of change is small for the majority of the diverging duct.

At the exhaust, the pressure graph (Graph 42.2) shows that the exhaust static gauge pressure of the gas is approximately zero which confirms that the nozzle is perfectly expanded as designed and expected. Some disturbance of the flow at the edges of the exhaust is observed. Caused simply by the geometry of the sharp corner, this is expected and considered insignificant. After the exhaust, another oblique shock is formed which is again expected and is due to the geometry of the exhaust boundary. Most nozzle flows are expected to generate shocks once outside the nozzle. This is typical for rocket nozzles and is also insignificant to the nozzle as they do not exert any forces on the nozzle wall – one of the reasons for in need of designing shock-free nozzles.

Conclusion

A procedure for designing axisymmetric rocket nozzles is presented. The analytically solvable iterative Axisymmetric MOC equations are implemented in a computer programme to increase the speed and accuracy of the design process. To obtain valid physical results from the procedure, isentropic calculations for nozzle flows are performed in order to iterate the MOC-generated nozzle to the isentropic exhaust radius. It is made clear that in reality the number of characteristic lines is infinite, however a finite amount is needed to be able to produce a nozzle contour. It is discovered that anything above 200 characteristic lines is suitable for accurate nozzle geometries and each of the slopes must be iterated at least 5 times to correct for the low accuracy of the compatibility equation solution. For this specific procedure, the nozzle wall contour is generated from the kernel as it is the only characteristic net that this paper focuses on constructing. This simplification of the model causes

additional issues such as the undefined transonic region which allows for the generation of oblique shock waves. To overcome this issue, a new boundary condition at the throat must be input to the problem and such boundary can be obtained from Sauer's transonic method. The length of nozzles produced with Axisymmetric MOC is also undesirable for a practical design. Ways of artificially truncating Axisymmetric MOC nozzles can be found to mitigate this issue. The irrotational and inviscid compatibility equations produce nozzles that are accurate only with certain theoretical models. For full-scale designs aiming to mimic physical nozzles corrections for variable chemical kinetics and viscous flows must be considered. The compatibility equations can be modified to account for such properties of the gas. Another approach to solving these issues is to use the generated inviscid contour as a benchmark geometry and perform additional calculations and optimizations to arrive at a more realistic model of a rocket nozzle.

References

1. Anderson, J. (2004) "Modern Compressible Flow: With Historical Perspective" 3rd Ed. New York: McGraw-Hill
2. Cumpsty, N. & Heyes, A. (2015) "Jet Propulsion" 3rd Ed. New York: Cambridge University Press
3. Reid, H. DeFrance, S. & Sharp, E. (1953) "Equations, Tables, and Charts for Compressible Flow: Report 1135". Moffett Field, CA: NACA
4. Hyde, J. & Gill, G. (1967) "Liquid Rocket Engine Nozzles: chemical propulsion." Cleveland: NASA
5. Huzel, D. & Huang, D. (1967) "Design of Liquid Propellant Rocket Engines" 2nd Ed. Washington, D.C.: NASA
6. McBride, B. & Gordon, S. (1996) "Computer Program for Calculation of Complex Chemical Equilibrium Compositions and Applications". Cleveland: NASA
7. Chatwin, C (2017), "Rocket Equation & Multistaging: Lecture for Satellite and Space Systems MSC" Sussex: University of Sussex
8. Taylor, T. (2009) "Introduction to Rocket Science and Engineering" Boca Raton: Taylor and Francis Group
9. Young, R. (2012) "Automated Nozzle Design through Axis-Symmetric Method of Characteristics Coupled with Chemical Kinetics" Auburn: Auburn University
10. Guentert, E. & Neumann, H. (1960) "Design of Axisymmetric Exhaust Nozzles by Method of Characteristics Incorporating a Variable Isentropic Exponent" Cleveland: NASA
11. Shapiro, A. (1953) "The Dynamics and Thermodynamics of Compressible Fluid Flow" Volume I. New York: John Wiley & Sons
12. Kulhanek, S. (2012) "Design, Analysis, and Simulation of Rocket Propulsion System" Kansas: University of Kansas

Appendices

Appendix A

The Axisymmetric MOC software can be found as an .exe and .py file. The .exe file can be used on a Windows7-10 OS and does not require any coding skills to use. The .py file is the source code and does require understanding of Python 3.7+. This file can be opened on any operating system.

The AXIMOC Nozzle Designer can be found on:

https://github.com/KyrilPalaveev/Axisymmetric-Method-of-Characteristics-Nozzle-Designer-with-GUI

Appendix B

Tabular Data for 2D Method of Characteristics for nozzle with 8 characteristic lines. Refer to the report for more information on this data.

deltatheta [deg]	v_e	first theta [deg]	gamma	M_e
5.0000	72.035	1.0175	1.1877	3.2554

Point	*K_ [deg]*	*K+[deg]*	*θ [deg]*	*ν [deg]*	*M*	*μ [deg]*
1	*2.035*	*0.000*	*1.018*	*1.018*	*1.077*	*68.166*
2	*12.035*	*0.000*	*6.017*	*6.017*	*1.269*	*51.979*
3	*22.035*	*0.000*	*11.017*	*11.017*	*1.422*	*44.670*
4	*32.035*	*0.000*	*16.017*	*16.017*	*1.565*	*39.724*
5	*42.035*	*0.000*	*21.017*	*21.017*	*1.703*	*35.963*
6	*52.035*	*0.000*	*26.017*	*26.017*	*1.840*	*32.926*
7	*62.035*	*0.000*	*31.017*	*31.017*	*1.977*	*30.381*
8	*72.035*	*0.000*	*36.017*	*36.017*	*2.117*	*28.193*
9	*72.035*	*0.000*	*36.017*	*36.017*	*2.117*	*28.193*
10	*12.035*	*-12.035*	*0.000*	*12.035*	*1.452*	*43.529*
11	*22.035*	*-12.035*	*5.000*	*17.035*	*1.593*	*38.883*
12	*32.035*	*-12.035*	*10.000*	*22.035*	*1.731*	*35.296*
13	*42.035*	*-12.035*	*15.000*	*27.035*	*1.868*	*32.373*
14	*52.035*	*-12.035*	*20.000*	*32.035*	*2.005*	*29.910*
15	*62.035*	*-12.035*	*25.000*	*37.035*	*2.145*	*27.783*
16	*72.035*	*-12.035*	*30.000*	*42.035*	*2.288*	*25.914*
17	*72.035*	*-12.035*	*30.000*	*42.035*	*2.288*	*25.914*
18	*22.035*	*-22.035*	*0.000*	*22.035*	*1.731*	*35.296*
19	*32.035*	*-22.035*	*5.000*	*27.035*	*1.868*	*32.373*
20	*42.035*	*-22.035*	*10.000*	*32.035*	*2.005*	*29.910*
21	*52.035*	*-22.035*	*15.000*	*37.035*	*2.145*	*27.783*

22	*62.035*	*-22.035*	*20.000*	*42.035*	*2.288*	*25.914*
23	*72.035*	*-22.035*	*25.000*	*47.035*	*2.435*	*24.247*
24	*72.035*	*-22.035*	*25.000*	*47.035*	*2.435*	*24.247*
25	*32.035*	*-32.035*	*0.000*	*32.035*	*2.005*	*29.910*
26	*42.035*	*-32.035*	*5.000*	*37.035*	*2.145*	*27.783*
27	*52.035*	*-32.035*	*10.000*	*42.035*	*2.288*	*25.914*
28	*62.035*	*-32.035*	*15.000*	*47.035*	*2.435*	*24.247*
29	*72.035*	*-32.035*	*20.000*	*52.035*	*2.586*	*22.745*
30	*72.035*	*-32.035*	*20.000*	*52.035*	*2.586*	*22.745*
31	*42.035*	*-42.035*	*0.000*	*42.035*	*2.288*	*25.914*
32	*52.035*	*-42.035*	*5.000*	*47.035*	*2.435*	*24.247*
33	*62.035*	*-42.035*	*10.000*	*52.035*	*2.586*	*22.745*
34	*72.035*	*-42.035*	*15.000*	*57.035*	*2.743*	*21.378*
35	*72.035*	*-42.035*	*15.000*	*57.035*	*2.743*	*21.378*
36	*52.035*	*-52.035*	*0.000*	*52.035*	*2.586*	*22.745*
37	*62.035*	*-52.035*	*5.000*	*57.035*	*2.743*	*21.378*
38	*72.035*	*-52.035*	*10.000*	*62.035*	*2.907*	*20.124*
39	*72.035*	*-52.035*	*10.000*	*62.035*	*2.907*	*20.124*
40	*62.035*	*-62.035*	*0.000*	*62.035*	*2.907*	*20.124*
41	*72.035*	*-62.035*	*5.000*	*67.035*	*3.077*	*18.966*
42	*72.035*	*-62.035*	*5.000*	*67.035*	*3.077*	*18.966*
43	*72.035*	*-72.035*	*0.000*	*72.035*	*3.255*	*17.889*
44	*72.035*	*-72.035*	*0.000*	*72.035*	*3.255*	*17.889*

Appendix C

Tabular Data for Axisymmetric Method of Characteristics for nozzle with 8 characteristic lines. Refer to the report for more information on this data.

K_ [deg]	K+ [deg]	θ [deg]	ν [deg]	M [-]	μ [deg]	V [m/s]	x [m]	r [m]	p [Pa]	T [K]
0.00	0.00	0.00	0.00	1.00	90.00	1211.35	0.00000	0.00000	4544907.66	3236.12
22.26	-22.26	0.00	22.26	1.74	35.16	1942.68	0.00000	0.01359		2760.49
29.02	-22.56	3.23	25.79	1.83	33.06	2025.58	0.00497	0.01715		2692.65
36.94	-23.13	6.90	30.03	1.95	30.86	2121.16	0.00816	0.01955		2610.92
42.95	-23.77	9.59	33.36	2.04	29.33	2193.83	0.01071	0.02156		2546.27
47.68	-24.47	11.61	36.08	2.12	28.18	2251.55	0.01312	0.02353		2493.35
51.50	-25.28	13.11	38.39	2.18	27.26	2299.86	0.01580	0.02578		2448.01
54.62	-26.27	14.17	40.44	2.24	26.50	2342.04	0.01917	0.02866		2407.64
54.62	-26.27	14.17	40.44	2.24	26.50	2342.04	0.00406	0.01568		
22.26	-22.26	0.00	22.26	1.74	35.16	1942.68	0.01929	0.00000	1656876.62	2760.49

36.01	-25.03	5.49	30.52	1.96	30.63	2131.96	0.02689	0.00573		2601.45
44.24	-28.04	8.10	36.14	2.12	28.15	2252.93	0.03239	0.00975		2492.07
50.63	-30.11	10.26	40.37	2.24	26.52	2340.55	0.03686	0.01306		2409.07
55.45	-31.77	11.84	43.61	2.33	25.38	2405.81	0.04084	0.01607		2345.21
59.06	-33.26	12.90	46.16	2.41	24.54	2456.21	0.04484	0.01913		2294.68
61.66	-34.74	13.46	48.20	2.47	23.90	2495.81	0.04936	0.02258		2254.24
61.66	-34.74	13.46	48.20	2.47	23.90	2495.81	0.04771	0.02133		
40.17	-40.17	0.00	40.17	2.23	26.60	2336.42	0.03857	0.00000	705465.90	2413.06
50.12	-42.23	3.94	46.17	2.41	24.53	2456.43	0.04675	0.00443		2294.45
56.14	-44.69	5.73	50.42	2.54	23.23	2538.26	0.05336	0.00805		2210.17
60.79	-46.45	7.17	53.62	2.63	22.31	2598.55	0.05927	0.01135		2146.31
64.12	-47.92	8.10	56.02	2.71	21.66	2642.79	0.06500	0.01462		2098.50
66.28	-49.24	8.52	57.76	2.76	21.20	2674.55	0.07114	0.01812		2063.68
66.28	-49.24	8.52	57.76	2.76	21.20	2674.55	0.09054	0.02920		
52.86	-52.86	0.00	52.86	2.61	22.53	2584.27	0.05786	0.00000	350818.62	2161.58
59.93	-54.32	2.80	57.13	2.74	21.37	2663.01	0.06643	0.00379		2076.38
64.10	-56.22	3.94	60.16	2.84	20.60	2717.70	0.07391	0.00718		2015.69
67.13	-57.60	4.76	62.36	2.92	20.06	2756.65	0.08109	0.01048		1971.72
68.92	-58.74	5.09	63.83	2.96	19.71	2782.31	0.08850	0.01390		1942.42
68.92	-58.74	5.09	63.83	2.96	19.71	2782.31	0.13915	0.03731		
61.74	-61.74	0.00	61.74	2.89	20.21	2745.62	0.07714	0.00000	203755.81	1984.25
66.50	-62.72	1.89	64.61	2.99	19.53	2795.78	0.08605	0.00344		1926.93
69.04	-64.08	2.48	66.56	3.06	19.09	2829.33	0.09432	0.00669		1888.01
70.48	-65.02	2.73	67.75	3.10	18.82	2849.65	0.10270	0.01000		1864.22
70.48	-65.02	2.73	67.75	3.10	18.82	2849.65	0.18746	0.04348		
67.63	-67.63	0.00	67.63	3.10	18.85	2847.66	0.09643	0.00000	138215.94	1866.56
70.39	-68.20	1.09	69.30	3.15	18.49	2875.72	0.10564	0.00323		1833.44
71.40	-69.00	1.20	70.20	3.19	18.29	2890.82	0.11467	0.00644		1815.49
71.40	-69.00	1.20	70.20	3.19	18.29	2890.82	0.22980	0.04719		
71.01	-71.01	0.00	71.01	3.22	18.12	2904.34	0.11571	0.00000	109503.24	1799.33
71.92	-71.20	0.36	71.56	3.24	18.00	2913.41	0.12522	0.00314		1788.44
71.92	-71.20	0.36	71.56	3.24	18.00	2913.41	0.26340	0.04901		
72.11	-72.11	0.00	72.11	3.26	17.89	2922.54	0.13500	0.00000	101325.00	1777.46
72.11	-72.11	0.00	72.11	3.26	17.89	2922.54	0.28926	0.04979		